ABSTRACT

Title of Thesis:	THE PERFORMANCE OF INTER-STORY ISOLATED STRUCTURES SUBJECT TO WIND AND EARTHQUAKE HAZARDS
	Kathleen Jane Russell Master of Science, 2018
Thesis Directed By:	Professor, Brian M. Phillips, Civil and Environmental Engineering

The implementation of inter-story isolation has gained popularity over the past decade. The focus of this thesis is to study the performance of an inter-story isolated building under earthquake ground motion as well as high wind forces through the time-history analysis of a multi-degree-of-freedom building model. The performance of the structure is compared to a conventional building with the same number of floors. Potential improvements to the inter-story isolation system are analyzed including the effects of varying the stiffness of the isolation layer, as well as adding viscous and rate-independent linear damping. Finally, practical methods of implementing rate-independent linear damping are discussed.

THE PERFORMANCE OF INTER-STORY ISOLATED STRUCTURES SUBJECT TO EARTHQUAKE AND WIND HAZARDS

by

Kathleen Jane Russell

Thesis submitted to the Faculty of the Graduate School of the
University of Maryland, College Park, in partial fulfillment
of the requirements for the degree of
Master of Science
2018

Advisory Committee:
Professor Brian M. Phillips, Chair
Professor M. Sherif Aggour
Professor Yunfeng Zhang

Acknowledgements

I would like to thank my advisor, Professor Brian M. Phillips, for his mentorship throughout my undergraduate and graduate studies at the University of Maryland. I am very grateful for the opportunity to experience international research collaboration at Tohoku University as an undergraduate, in addition to Professor Phillips' insight and advice throughout my studies.

I would like to thank Professor M. Sherif Aggour and Professor Yunfeng Zhang, for the time they have taken to be on the advisory committee and provide feedback.

I also would like to express my appreciation to my family and friends who have supported me over the course of my education, and especially with my graduate studies. My parents, Dan and Tina Russell, and grandmother, Maria Festa, have always encouraged and supported me to pursue education as a route to success, and I would not be where I am today without them. I am also very grateful for the support and sacrifices from my sisters, Teresa, Kristen, Danielle, Jenna, and Mary Russell, throughout this process. Finally, I would like to thank my fiancé, Michael Whiteman, for his love, encouragement, and understanding.

Table of Contents

List of Tables

List of Figures

Chapter 1: Introduction

1.1 Background and Motivation

Natural hazards cause numerous design concerns for civil infrastructure, including life safety and the integrity of the structure under extreme events and occupant comfort and structural fatigue under frequent events. Commonalities across major disasters include property and infrastructure damage, displaced populations, and loss of life. The death and injury tolls from these events vary based on several factors, such as time of day, and population density (Alexander and Alexander 2011). Certain geographic regions are more prone to certain events, like earthquakes or strong winds, and infrastructure must be designed accordingly.

If a structure is located in an area with seismic activity but is inadequately designed to handle a seismic event, it needlessly heightens the risk of collapse, which in turn puts the building occupants, as well as those in the vicinity of the building, at risk of injury or death. This becomes a larger threat when frequent seismic activity coincides with urban populations; such is the case with Tokyo and Istanbul (Alexander 2011). Major wind events such as hurricanes, tropical storms, and tornados, also create circumstances that can damage structures, and in turn, threaten life safety of a community. Uncharacteristic loads from wind gusts can affect the load capacity of a building. Even in the circumstances that a structure survives such an event, large displacements and accelerations can damage the non-structural components and contents of the building (Anajafi and Medina 2017). Additionally, debris and broken glass can harm people inside and outside of the building. More

frequent wind events may not damage a building, but can lead to occupant discomfort and a temporary loss of function for the building.

Earthquake and strong wind events rarely occur simultaneously, but there are regions that are vulnerable to both hazards. Figure 1.1 visualizes which areas of the United States are prone to certain types of natural hazards. It is apparent that, especially in the Midwest and Mid-Atlantic, there are regions which are susceptible to both earthquakes and strong wind events. Properly designing a building to withstand the geographically relevant natural hazards is imperative to prioritize and protect public health and safety, the primary aim of the civil engineering profession according to the American Society of Civil Engineers' Code of Ethics (Vesilind 1995). There are many more regions worldwide which must design for strong seismic and wind loads, including Japan, Taiwan, and some regions of China.

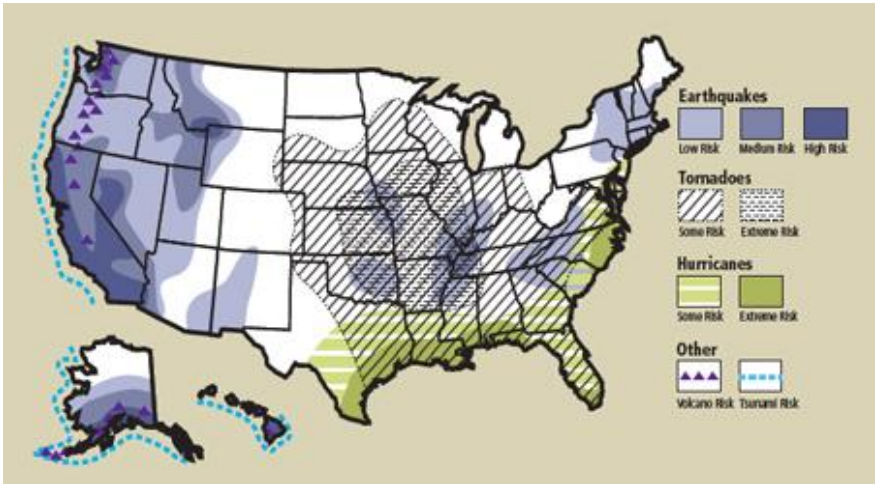

Figure 1.1 Risk of Natural Hazard to United States by Severity and Region (Duwadi and Muleny 2012)

Implementation of inter-story isolation systems as a protective system against earthquake damage is a fairly recent phenomenon that is gaining traction, due in part to research accomplishments and successful practical implementation. These systems

provide a means to protect the structural integrity of a building, and are a more feasible retrofit option than base-isolation, particularly in dense urban environments (Wang et al. 2012). Installing the isolation layer on the roof of a building can allow additional floors to be constructed above the original structure without significantly increasing the base shear. Inter-story isolation as a retrofit option avoids the risks and costs associated with foundation excavation (i.e., to install base isolation or increase base shear capacity). Also, because the additional floors are isolated from the original structure, they can be constructed with more cost-effective building materials, different geometry, or intended use. The use of materials other than the original building material for an addition generally creates complex dynamic behavior. Separating an addition by means of inter-story isolation creates a system where the dynamic behavior can be modeled relatively simpler. Further, minimally-disruptive retrofit construction methods are being developed for inter-story isolation systems (Ryan and Earl 2010). Shake table real-time hybrid simulation tests have been used to verify numerical simulations and develop supplemental control systems for the isolation layer (Zhang et al. 2017).

Examples of inter-story isolated construction to mitigate earthquake response in mid-rise and high-rise buildings can be found throughout the world. In Japan, the Iidabashi First Building, Koraku 2-Chome Building and Shidome Sumitomo Building are examples of functional inter-story isolated buildings (Sueoka 2004).

The goal of this thesis is to explore the use of inter-story isolation as a protective system for both earthquake and wind hazards. There are a handful of studies related to earthquake performance, but little available on the wind

performance of inter-story isolation. A comparison between a standard retrofit and an inter-story isolated retrofit gives insight to the dynamic behavior of conventional construction and inter-story isolation relative to the original structure. The Iidabashi First Building in Tokyo, Japan is used as a baseline to create the three structural models for evaluation under different loading scenarios. Supplemental damping added to the isolation layer will be evaluated for further improvement the system's performance under earthquake and wind.

1.2 Overview

The focus of this thesis is the performance of an inter-story isolated building under dynamic loading from both earthquakes and wind. The performance of the structure was compared to a conventional continuous structure with the same number of floors. The effects of varying the stiffness of the isolation layer was also analyzed. Subsequently, supplemental viscous and rate-independent linear damping was added to the inter-story isolated structure so as to further reduce displacements. Finally, practical methods of implementing these forms of damping are discussed.

Chapter 2 reviews previous studies related to inter-story isolation. The major differences between base isolation and inter-story isolation is explained, and the concept of utilizing the superstructure as a tuned mass damper is explored. The concept and implementation of rate-independent linear damping as a more effective method to provide supplemental damping to inter-story isolation systems is also covered.

Chapter 3 outlines the model parameters and methodology used in the dynamic analysis of the structure. Details about the structure being modeled, the

Iidabashi First Building, are presented. The creation of original and retrofit structures based on the Iidabashi First Building are discussed. The earthquake ground motions selected and the processing of wind tunnel data for use in numerical simulations is also discussed.

Chapter 4 covers the performance of inter-story isolation in different loading situations without additional damping devices. The response of the original 9-story building model will be compared to the responses of two retrofit scenarios. The first scenario supposes that 5 additional stories were constructed on top of the original structure using conventional construction and no isolation. The second scenario supposes the same addition is constructed using inter-story isolation between floors 9 and 10.

Chapter 5 focuses on improving the performance of the inter-story isolated structure through supplemental damping and increased isolation layer stiffness. A theoretical analysis in the frequency domain is used to compare the performance of viscous damping to rate-independent linear damping (RILD). The idea of tuning the superstructure to a tuned mass damper is also explored.

Chapter 6 focuses on replicating the non-causal RILD behavior in the time domain. A time-dependent implementation of damping is desired in order to respond to these hazards in a realistic scenario.

Chapter 7 summarizes the conclusions and findings of this paper, and provides recommendations for future study.

Chapter 2: Literature Review

2.1 Isolation Systems

2.1.1 Base Isolation

Base isolation is a protective system implemented at the foundation of a structure to reduce the response of the structure to earthquake excitation. A low-stiffness "isolation layer," usually consisting of flexible rubber bearings, separates the structure from the ground. The isolation layer reduces the fundamental natural frequency of the structure, reducing the inter-story drift and acceleration of the floors above (Anajafi and Medina 2017). The trade-off is that the low-stiffness of the isolation layer produces large displacements at the isolation layer, most notably in the first mode shape of the structure (Ryan and Earl 2010). Dampers are generally added to reduce these displacements, but base-isolated buildings still require specially-designed foundations and utility connections to accommodate significant displacements. This can create problems for mid-rise and high-rise buildings in cities as larger overturning moments and loads on the isolation bearings increase the risk of damage to the isolators (Anajafi and Medina 2017). In addition, base isolation is not an effective system for reducing wind-induced vibrations, which are a more prominent concern for mid-rise and high-rise buildings. Base isolation is most effective when the excitation occurs below the isolation layer, so that the isolators and any additional dampers can dissipate energy of the input excitation, thereby reducing the response of the upper stories. In the case of the wind load, forces are applied at each story of the building, which means energy is entering the system above the isolation layer and is not filtered by the isolation layer. Inter-story isolation provides

an alternative protective system for mid-rise and high-rise buildings by achieving the benefits of base-isolation with potential applications to protection against wind-induced vibration (Anajafi and Medina 2017).

2.1.2 Inter-Story Isolation

Inter-story isolation is similar to base isolation in that a low-stiffness layer separates the structure above it from the contents below. For inter-story isolation, however, one or more stories of the structure exist below the isolation layer (the substructure). By reducing the stiffness at the isolation layer, the fundamental natural frequency of the total structure is decreased, and the structure above the isolation layer (the superstructure) acts similarly to a base-isolated structure, experiencing significantly lower accelerations than a conventionally-constructed building of the same height and weight.

The main application of inter-story isolation has been to reduce the acceleration of the floors above the isolation layer when a structure experiences earthquake ground motion (Tan et al. 2008). The isolation layer effectively absorbs energy from the earthquake input. It “filters” the ground motion by separating the superstructure from the substructure, only allowing the absolute acceleration of the floor below, not the ground motion itself, to excite the superstructure.

The deformation of the isolation layer is evident for at least the first few damping modes. Additionally, the deformation and shear of the isolation layer increases as the height of the installation location increases (Wang et al. 2012). Because of the excessive displacement at this location, installing dampers is a

common practice to comply with deformation limits set by building codes and isolator manufacturers, and to reduce the threat of collision with nearby buildings.

2.2 Supplemental Control in Inter-Story Isolated Structures

2.2.1 Tuned Mass Damper

A tuned mass damper (TMD) is used to increase the damping of the structure (Housner et al. 1997). The function of a TMD is primarily to reduce acceleration of a building and dissipate vibrations faster than an uncontrolled system so as to prevent structural damage (Liu et al. 2008). A TMD is used most often in the context of reducing wind-related vibrations; however, a major drawback of these devices is that they have large displacements, which may cause them to collide with their surroundings. Traditional TMDs are vibrating masses encapsulated in the top of a building and tuned to match the fundamental natural frequency of the building. As an alternative to adding TMD mass to a structure, existing mass can be employed. A recent study from the University of New Hampshire concluded that by isolating a percentage of the total building mass, thereby creating a partial mass isolation (PMI) system, effectively combines the benefits of a TMD and base isolation system for seismic design, which is especially useful in the context of high-rise buildings (Anajafi and Medina 2017). By isolating portions of a building's mass, more desirable dynamic responses can be attained. The idea of PMI can be extended to inter-story isolation systems, creating a superstructure that is tuned to the natural frequency of the substructure. This system has the potential to both dissipate energy effectively and reduce the base shear demands on the building foundation.

Researchers from Universitá di Roma explored the concept of using the upper stories of an inter-story isolation system as an unconventional TMD (Reggio and De Angelis 2015). They present an energy-based design method for inter-story isolation and compare its performance under earthquake excitation. By analyzing a five-degree-of-freedom model, they were able to conclude that the inter-story drift of each floor, except for the isolation layer, along with the absolute acceleration of each floor decreased by about 45-50% on average. However, it was noted that the seismic performance of the system depends on several parameters, including the vertical location of the isolation layer, the frequency of the input ground motion, and which response parameter is compared.

2.1.2 Rate-Independent Linear Damping

As mentioned previously, large displacements are a point of concern when implementing inter-story isolation systems. Hybrid inter-story isolation systems have been implemented (Feng 1993) to combat this issue. Installing discrete dampers to the isolation layer allows more energy to be dissipated at the isolation layer and reduces its peak displacement. Viscous dampers effectively reduce floor displacement, but increase floor acceleration. Floor acceleration dictates the comfort level of building occupants (Zhou et al. 2003), and is considered a serviceability constraint for wind vibration control in building codes such as ASCE 7-10 (ASCE 2010). Additionally, under low-frequency inputs, viscous damping is much less effective because the damping force is dependent on velocity (Sagami et al. 2012). A low-frequency input has a lower velocity, which in turn creates a lower viscous damping force and reduces the effectiveness of viscous damping to reduce the response of a structure. Rate-

independent linear damping (RILD) is considered here as an alternative to viscous damping due to the fact that it is proportional to displacement (advanced in phase $\pi/2$ radians) rather than velocity, and its ability to reduce the response of a structure under a wider range of input frequencies.

RILD is a theoretical damping model that is frequency independent. Because the applied force is proportional to the displacement advanced in phase $\pi/2$ radians, RILD is non-causal. Because RILD is non-causal the simplest method to analyze the response of a system with RILD is in the frequency domain. There are causal models that mimic RILD and can be used in time domain analyses, including a causal, filter-based method (Keivan 2017) which will be considered for this study.

RILD is particularly beneficial in improving the performance of low-frequency structures which experience ground excitation at a frequency higher than the natural frequency of the structure (Keivan 2017). A practical, causal application of this theoretical damping was successfully implemented on a base isolated structural model. By using the filter-based method and a semi-active controller for a magneto-rheological damper, the researchers were able to closely imitate the ideal non-causal RILD. This creates a potential improvement to inter-story isolation as a protective system, as the isolated superstructure behaves as a low-frequency structure subject to high-frequency excitations.

Chapter 3: Methodology

3.1 Model and Parameters

The structure modeled for this research is the Iidabashi First Building in Tokyo, Japan (Figures 3.1-3.2). This building comprises of 14 stories, 5 of which sit atop an isolation layer consisting of 800-mm diameter lead rubber bearing isolators. The scenario created for this study is a comparison of retrofit options. The "original structure" was assumed to be the substructure of the building, (i.e. a 9-story structure), with the final structure containing a 5-story addition. For the initial performance analysis of the building's response under earthquake and wind excitation, the original structure was compared to the response of two retrofit options.

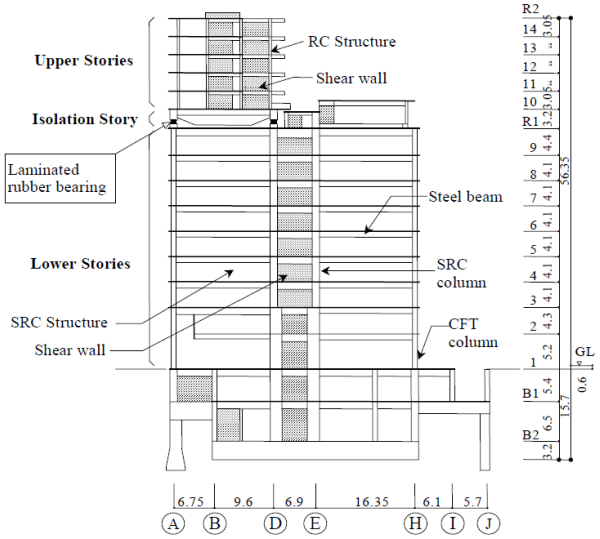

Figure 3.1 Building Elevation View (Murakami et al. 2008)

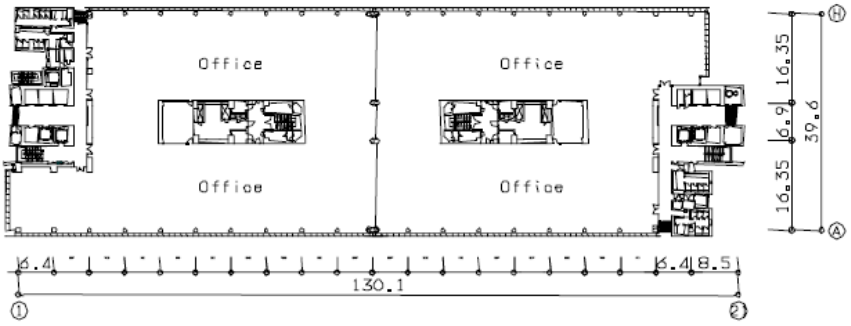

Figure 3.2 Building Plan View (Murakami et al. 2008)

The first retrofit option is a standard retrofit addition of 5 floors on the roof of the original structure, while the second option includes an isolation layer between the roof of the 9-story building and the 5-floor addition. Each of the three structures considered can be modeled as a lumped mass model containing *n* degrees of freedom (DOF). This results in a 9-DOF model for the original structure (Figure 3.3a), a 14-DOF model for the first retrofit option (Figure 3.3b), and a 15-DOF model for the second retrofit option (Figure 3.3c). The isolation layer has its own mass and stiffness, thereby creating an additional dynamic degree of freedom when compared to a conventional structure. The 15-DOF model was then used to analyze potential performance improvements upon inter-story isolation.

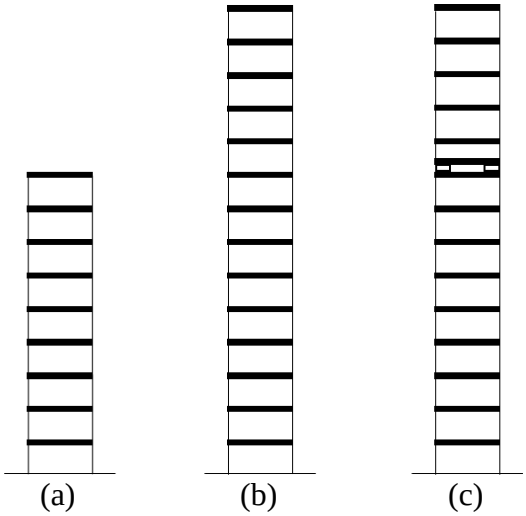

Figure 3.3 Analysis Structures (a) 9-DOF (b) 14-DOF (c) 15-DOF

Each DOF has a corresponding value of mass, stiffness, and damping. The structural properties can be represented by the following matrices, where *n* is the number of degrees of freedom of each model.

$$\boldsymbol{M} = \begin{bmatrix} m_1 & 0 & 0 & 0 \\ 0 & m_2 & 0 & 0 \\ 0 & 0 & \ddots & \vdots \\ 0 & 0 & \cdots & m_n \end{bmatrix} \qquad \boldsymbol{K} = \begin{bmatrix} k_1 + k_2 & -k_2 & 0 & 0 \\ -k_2 & k_2 + k_3 & -k_3 & \vdots \\ 0 & -k_3 & \ddots & -k_n \\ 0 & \cdots & -k_n & k_n \end{bmatrix}$$

$$\boldsymbol{C} = \begin{bmatrix} c_1 + c_2 & -c_2 & 0 & 0 \\ -c_2 & c_2 + c_3 & -c_3 & \vdots \\ 0 & -c_3 & \ddots & -c_n \\ 0 & \cdots & -c_n & c_n \end{bmatrix}$$

The values that populate the M, K, and C matrices for each model are tabulated in Tables 3.1a-3.1c. The mass is assigned as a lumped mass to the floor (DOF) identified while stiffness and damping are between the floor identified and the floor below. The values used for the 15-DOF structure are the same as those used by Murakami et al. (Murakami et al. 2008). For consistency in comparison, Rayleigh damping of 5% and 4% was assigned for the first two modes, respectively, for the two other models. For the earthquake and wind loads considered, interstory drifts remained less than 2% (excluding the isolation layer). For simplicity, a linear model is used.

Table 3.1 Structural Properties (a) 9-DOF (b) 14-DOF (c) 15-DOF

(a)

Floor/Degree of Freedom n	Mass m_n (10^6 kg)	Stiffness k_n (10^6 kN/m)	Damping c_n (10^3 kN*s/m)
1	5.4347	12.303	49.468
2	5.5328	12.814	50.257
3	5.2091	10.961	42.989
4	5.1895	9.8208	38.518
5	5.1797	9.1243	35.787
6	5.0914	8.5484	33.528
7	4.9148	7.9608	31.223
8	4.9148	7.4595	29.257
9	12.7040	7.1672	28.111

(b)

Floor/Degree of Freedom n	Mass m_n (10^6 kg)	Stiffness k_n (10^6 kN/m)	Damping c_n (10^3 kN*s/m)
1	5.4347	12.303	54.967
2	5.5328	12.814	47.018
3	5.2091	10.961	42.128
4	5.1895	9.8208	39.140
5	5.1797	9.1243	36.670
6	5.0914	8.5484	34.149
7	4.9148	7.9608	31.999
8	4.9148	7.4595	30.745
9	12.7040	7.1672	147.68
10	2.3152	34.426	98.134
11	2.3152	22.877	86.276
12	2.3054	20.112	71.152
13	2.3054	16.587	40.457
14	1.6579	9.4313	40.786

(c)

Floor	Degree of Freedom n	Mass m_n (10^6 kg)	Stiffness k_n (10^6 kN/m)	Damping c_n (10^3 kN*s/m)
1	1	5.4347	12.303	133.39
2	2	5.5328	12.814	138.52
3	3	5.2091	10.961	118.48
4	4	5.1895	9.8208	106.16
5	5	5.1797	9.1243	98.632
6	6	5.0914	8.5484	92.407
7	7	4.9148	7.9608	86.055
8	8	4.9148	7.4595	80.636
9	9	12.7040	7.1672	77.476
Isolation Layer	10	4.0221	0.052974	0.57264
10	11	2.3152	34.426	372.14
11	12	2.3152	22.877	247.30
12	13	2.3054	20.112	217.41
13	14	2.3054	16.587	179.30
14	15	1.6579	9.4313	101.95

Using the tabulated structural properties, the dynamic properties of each model can be calculated. The natural frequencies of each mode can be found using the following equation, where *det* indicates the determinate.

$$det[\boldsymbol{K} - \omega^2 \boldsymbol{M}] = 0 \qquad (3\text{-}1)$$

The first 5 natural frequencies and mode shapes are expressed in Table 3.2 and Figures 3.4-3.6. The low-stiffness isolation layer of the 15 DOF model creates a low frequency mode, lower than first modal frequency of the 9-DOF structure. When the first mode is excited by some input to the system, the response will be concentrated in the isolation layer (Figure 3.6) and significantly reduce inter-story drift of all other floors when compared to the original structure and standard retrofit option.

Table 3.2 First Five Natural Frequencies of Structural Models

Mode	Frequency (Hz)		
	9-DOF	14-DOF	15-DOF
1	1.02	0.86	0.29
2	2.93	2.67	1.05
3	4.95	4.64	2.93
4	6.92	6.03	4.95
5	8.76	7.07	6.92

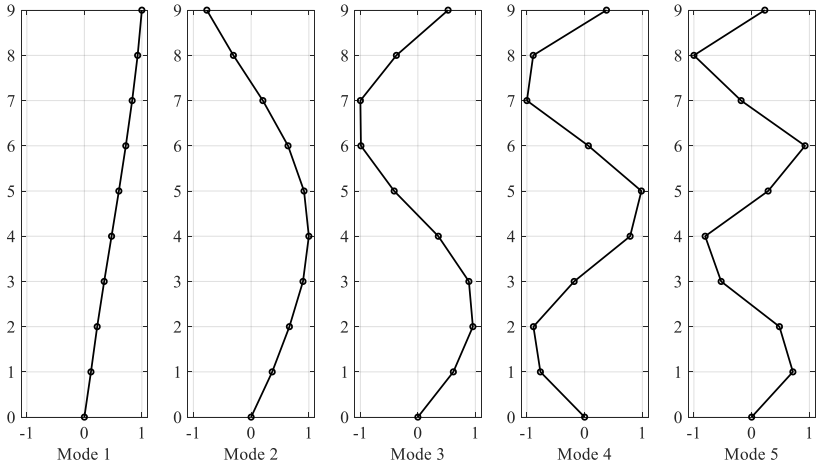

Figure 3.4 First Five Mode Shapes of 9-DOF Model

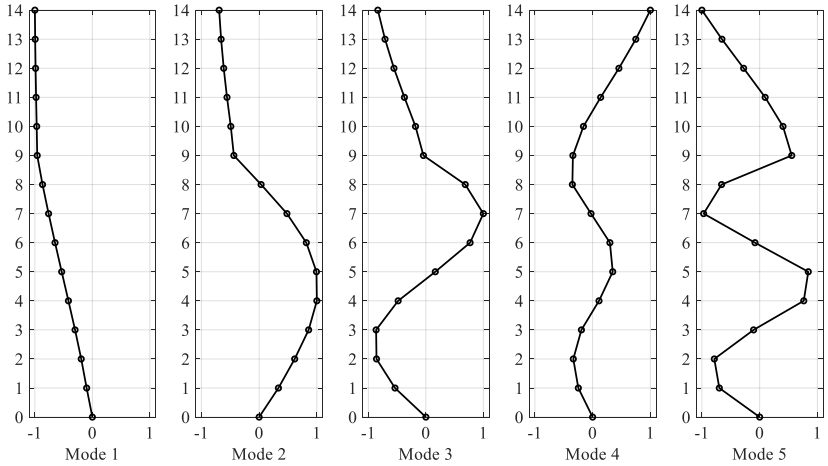

Figure 3.5 First Five Mode Shapes of 14-DOF Model

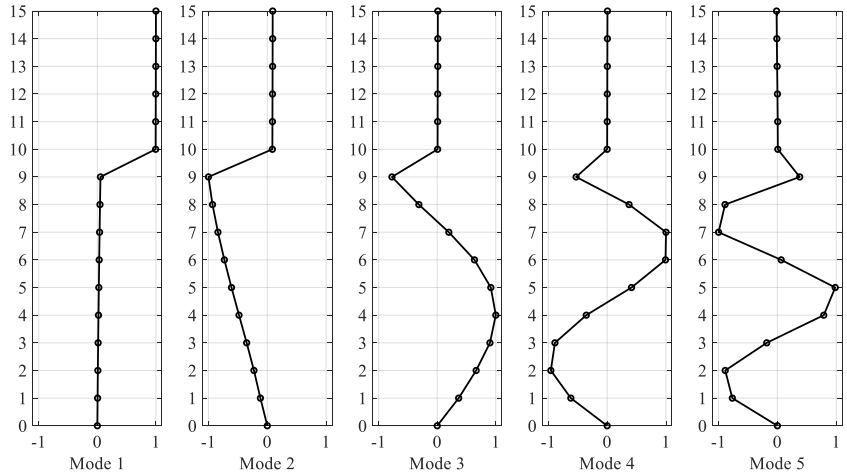

Figure 3.6 First Five Mode Shapes of 15-DOF Model

3.2 State Space

A generalized equation of motion can be composed for each of the two loading types explored in this paper. The equation of motion for a dynamic system undergoing earthquake excitation $\ddot{x}_g$ can then be written as

$$\boldsymbol{M}\ddot{x} + \boldsymbol{K}\dot{x} + \boldsymbol{C}x = -\boldsymbol{M}\ddot{x}_g \tag{3-2}$$

The equation of motion for a dynamic system undergoing wind excitation $F(t)$ can be written as

$$\boldsymbol{M}\ddot{x} + \boldsymbol{K}\dot{x} + \boldsymbol{C}x = \boldsymbol{F}(t) \tag{3-3}$$

Where the input force F contains *n* forces, one for each DOF, at each time step. To efficiently evaluate the three structural models under various conditions, each was represented and evaluated using state space. With the use of numerical simulation, all of the structures can be modeled and analyzed in a matter of seconds. By assuming a linear system, the following state space equations are valid.

$$\dot{\boldsymbol{x}} = \boldsymbol{A}\boldsymbol{x} + \boldsymbol{B}\boldsymbol{u} \tag{3-4}$$

$$\boldsymbol{y} = \boldsymbol{C}\boldsymbol{x} + \boldsymbol{D}\boldsymbol{u} \tag{3-5}$$

Where $\boldsymbol{x}$ is the state vector, $\boldsymbol{y}$ is the output vector, $\boldsymbol{u}$ is the input vector, $\boldsymbol{A}$ is the system matrix, $\boldsymbol{B}$ is the input matrix, $\boldsymbol{C}$ is the output matrix, and $\boldsymbol{D}$ is the feedthrough or zero matrix. The $\boldsymbol{A}$, $\boldsymbol{B}$, $\boldsymbol{C}$, and $\boldsymbol{D}$ matrices are composed of the system mass, stiffness, and damping properties ($\boldsymbol{M}$, $\boldsymbol{K}$, and $\boldsymbol{C}$). The state space matrices can then be defined as the following matrices for an earthquake ground motion, with structure with n degrees of freedom, with $\mathbf{0}$ referring to an $n \times n$ zero matrix and $\boldsymbol{I}$ referring to an $n \times n$ identity matrix. In this case, the input vector u is a ground acceleration.

$$\boldsymbol{A} = \begin{bmatrix} \mathbf{0} & \boldsymbol{I} \\ -\boldsymbol{M}^{-1}\boldsymbol{K} & -\boldsymbol{M}^{-1}\boldsymbol{C} \end{bmatrix}_{2n\,x\,2n} \qquad \boldsymbol{B} = \begin{bmatrix} \mathbf{0} \\ -\boldsymbol{\Gamma} \end{bmatrix}_{2n\,x\,1} \qquad \boldsymbol{\Gamma} = \begin{bmatrix} \mathbf{1} \\ \vdots \\ \mathbf{1} \end{bmatrix}_{n\,x\,1}$$

$$\boldsymbol{C} = \begin{bmatrix} \boldsymbol{I} & \mathbf{0} \\ \mathbf{0} & \boldsymbol{I} \\ -\boldsymbol{M}^{-1}\boldsymbol{K} & -\boldsymbol{M}^{-1}\boldsymbol{C} \end{bmatrix}_{3n\,x\,2n} \qquad \boldsymbol{D} = \begin{bmatrix} \mathbf{0} \\ \mathbf{0} \\ \mathbf{0} \end{bmatrix}_{3n\,x\,1}$$

To represent wind loading on a structure, the input vector u changes, thus changing the composition of the $\boldsymbol{B}$ and $\boldsymbol{D}$ matrices. The input vector contains a force input to each DOF and must be multiplied by the mass matrix of the system in order to convert it from forces to accelerations. Thus, the following $\boldsymbol{B}$ and $\boldsymbol{D}$ matrices are produced.

$$\boldsymbol{B} = \begin{bmatrix} \mathbf{0} \\ -\boldsymbol{M}^{-1} \end{bmatrix}_{2n\,x\,n} \qquad \boldsymbol{D} = \begin{bmatrix} \mathbf{0} \\ \mathbf{0} \\ -\boldsymbol{M}^{-1} \end{bmatrix}_{3n\,x\,n}$$

3.3 Simulation Set-up

The state space model of each structure was evaluated in MATLAB r2018a using Simulink to perform time history analysis and built-in functions to perform

frequency domain analysis (MATLAB 2018). The initial performance analyses in Chapter 4 used Simulink for time domain analysis. The viscous and RILD supplemental damping analyses in Chapter 5 were evaluated in the frequency domain. RILD is non-causal and easiest to model in the frequency domain. Viscous damping was also evaluated using the frequency domain for consistency when comparing to RILD. The causal model for RILD used in Chapter 6 was evaluated in a Simulink time domain analysis and compared to the RILD frequency domain analysis.

In the time domain analysis, a fourth order Runge-Kutta numerical integration algorithm was used to evaluate both earthquake and wind responses. The earthquake time histories were about 60 seconds each, and were analyzed with a 1/2000 second sampling time. For the wind load, the time history analysis was approximately 42 minutes long, sampled at 25 Hz, and analyzed using a sampling time of 1/1000 seconds. The state space model was evaluated at each time step and the displacement, velocity, and acceleration of each degree of freedom were recorded.

In the frequency domain analysis, a Fourier Transform of each input force was performed using the "fft" command in Matlab. The input was shifted to be between half the sampling frequency, ±1000 Hz for the earthquake loads and ±12.5 Hz for the wind load, to accommodate the idiosyncrasies of the "fft" command. The frequency response of the state space system was then calculated over the same frequency range and multiplied by the input at each frequency. The frequency was then shifted back to the original range (0 to the sampling frequency) and the inverse Fourier Transform ("ifft" command) was used to produce the time histories of the displacement, velocity, and acceleration time histories for each degree of freedom.

3.4 Earthquake Time Histories

The three model structures were each subjected three full-scale earthquake ground motions (Figure 3.7). These time histories were selected from the benchmark study (Ohtori et al., 2004) and contain various frequency content and magnitudes: The N-S component recorded at the Kobe Japanese Meteorological Agency (JMA) station during the Hyogo-ken Nanbu earthquake of January 17, 1995; the N-S component recorded at the Imperial Valley Irrigation District substation in El Centro, California, during the Imperial Valley, California earthquake of May 18, 1940; and the N-S component recorded at Sylmar County Hospital parking lot in Sylmar, California, during the Northridge, California earthquake of January 17, 1994. Note that the full earthquake records were used in analyses. The inter-story drifts observed under these earthquakes were consistently under 2%. Because significant nonlinear response is not expected at this level of drift, all analyses were run using linear models.

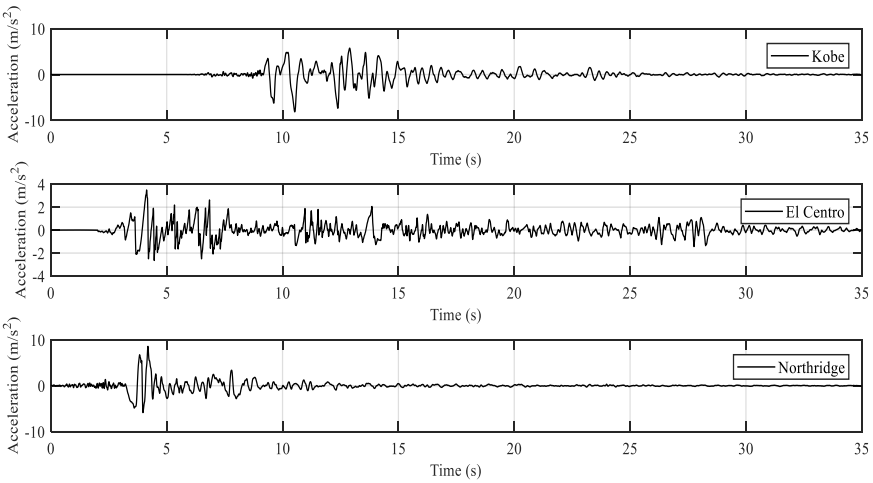

Figure 3.7 Earthquake Time History Data

3.5 Processing of Wind Loading

The time history data used to create the wind forces applied to the models is from the Tokyo Polytechnic University Aerodynamic Database (Tamura 2012). The aspect ratio available in the "Wind Pressure Database for High-Rise Building" that was most similar to the actual structure was used for an approximation of realistic wind pressure coefficient (C_p) values. Therefore, the model of dimensions 0.3m × 0.1m × 0.2m (120m × 40m × 80m full-scale) was selected. Figure 3.8 is an "unfolded" view of the wind tunnel model, showing taps on all envelope wall surfaces. The wind direction selected was a force perpendicular to the long side of the building so that the wind analysis occurs along the same plane as the earthquake analysis. This causes pressure on the windward face and suction on the leeward face of the building. Only the along-wind loading and response were considered.

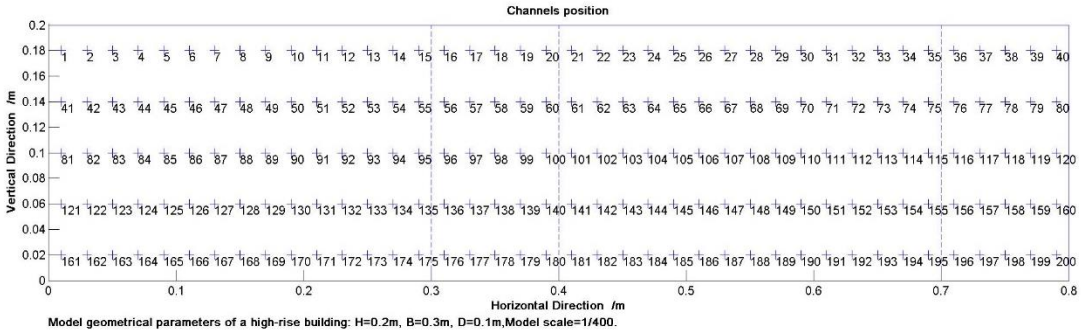

Figure 3.8 Wind Tunnel Model with Dimensions and Tap Locations (Tamura 2012)

The C_p values from the taps on the leeward face of the building were subtracted from those from the windward building to account for how the wind force affects the entire structure once it is simplified into a 9, 14, or 15 DOF lumped-mass model. The tributary area of each tap is equal, so the average C_p value for each horizontal row of taps is taken to condense the 75 windward and leeward taps down to 5 effective inputs along the height. The tributary area of each of these 5 taps equals

1/5 the total building area, which can then be cross-referenced with the tributary area of the each dynamic DOF to allot a weighted average of C_p to each DOF based on how much of the tributary areas overlap each other. The C_p values were scaled according to the method outlined by Pierre et al. (2005). The simplified equation to obtain GC_p is expressed below, with E_C/K_h referring to a factor related to the building's exposure and roof height.

$$GC_p = \frac{E_C}{K_h}\left(\frac{1}{1.52}\right)^2 \tag{3-6}$$

The pressure on each DOF was then calculated in accordance with ASCE 7-10 equations 27.3-1 and 27.4-1 using a strength-level, 3-second gust wind speed V of 54 m/s, which has a return period of 50 years (ASCE 2010).

$$P_n = 0.613V^2 * GC_p \tag{3-7}$$

The force on each DOF was then calculated using equation 3-6 where $\boldsymbol{P_n}$ is the time history of the pressure on DOF n, $\boldsymbol{A_n}$ is the area of DOF n, and F_n is the time history of the force.

$$F_n = \frac{P_n}{A_n} \tag{3-8}$$

The TPU database presents time histories of wind pressure coefficient data for each tap over a span of 32.7 seconds. Converting the model-scale data to full scale is twofold: the time over which the force occurs must be scaled along with the C_p values. The model-scale and full-scale time can be related through similitude using the model-scale and full-scale frequency.

$$\left(\frac{fL}{v}\right)_m = \left(\frac{fL}{v}\right)_f \tag{3-9}$$

Where *m* denotes model scale and *f* denotes full scale. The median wind speed for the wind tunnel data (10.93 m/s) is to be used as v_m and the design wind speed in accordance with ASCE 7-10 (54 m/s) is to be used for v_f. The sample frequency is given as 1000 Hz, and the scale (L_m/L_f) is 1/400. This yields a value of f_f = 12.35 Hz, or a time step of 0.081 seconds. Scaling of the time vector then produces a time history of approximately 42 minutes. Because the sampling frequency of the wind load is similar to the frequency of higher modes of the 14-floor structures, the load was resampled to have a sampling frequency of 25 Hz.

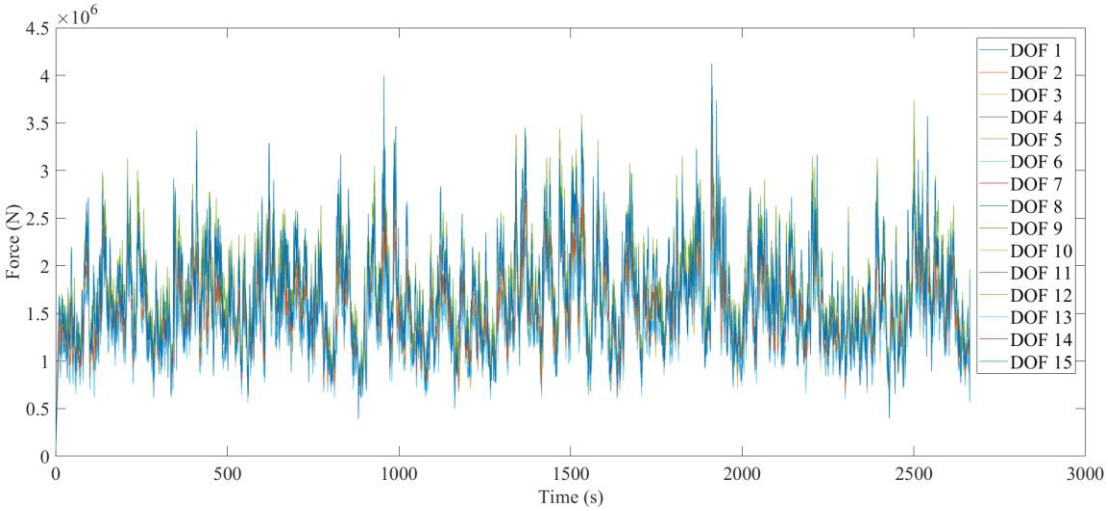

Figure 3.9 Full Scale Wind Force (15 DOF)

All tabulated values from wind analyses in Chapters 4, 5, and 6 are the results of Gumbel extreme value analysis, in which the statistical probability of non-exceedance is taken into consideration (Gavanski et al. 2016). A Fisher-Tippett Type I (Gumbel) distribution, a standard distribution in wind engineering, was used to divide each DOF response time history into 50 equal sections. The maximum and minimum values were taken from each section, and the 78th percentile of the resulting distribution was used to estimate the maximum and minimum response. The

maximum of the absolute value of the two response values was taken to be the peak response.

Chapter 4: Performance Analysis

4.1 Overview

To analyze inter-story isolation as a multi-hazard protective system, the three models (Figure 3.3) were independently subjected to three earthquake time histories and the wind time history derived from a BLWT test. The 9-DOF model refers to the original structure, 14-DOF model refers to the standard retrofit, and 15-DOF model refers to the inter-story isolated retrofit, as pictured in Figure 3.3. Inter-story isolation is generally designed to improve seismic performance of a structure. Analyzing its performance in high-wind scenarios compared to the performance of a standard retrofit will give insight into the practicality of using inter-story isolation as a retrofit technique in geographic regions with both earthquake and wind-related hazards. For each loading scenario, the performance of each structure was compared based on the maximum accelerations and base shear.

4.2 Earthquake Load Analysis

The time history responses of each of the three model structures for the Northridge earthquake are presented in Figures 4.1-4.3. Tables 4.1a-4.1c include the results for all earthquakes considered. The base shear of the inter-story isolated structure remained comparable to the original 9-story structure. This result suggests that in an inter-story isolation retrofit scenario, the original building foundation may not need to be heavily redesigned to accommodate a large increase in shear force. Similar results are seen for the standard retrofit building. In this case, the decrease in natural frequency keeps the base shear low, comparable to the original 9-story structure. The most significant improvement across all cases is the reduction of the

acceleration of the superstructure through inter-story isolation. As shown in Figure 4.3, the acceleration of 10^{th}-14^{th} stories overlap and are much lower than the accelerations of the substructure. In the standard retrofit case, the acceleration continues to increase along the height of the building. By adding inter-story isolation between the 9^{th} and 10^{th} stories, the isolation layer essentially causes the superstructure to act as a base-isolated structure with the input acceleration coming from the floor below. This results in an approximately 80-85% reduction in the acceleration of the 14^{th} floor when compared to a standard retrofit of the same dimensions.

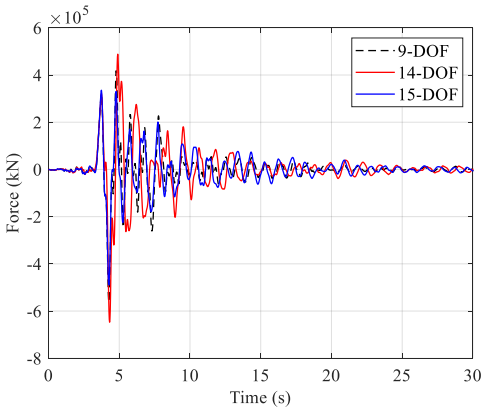

Figure 4.1 Base Shear

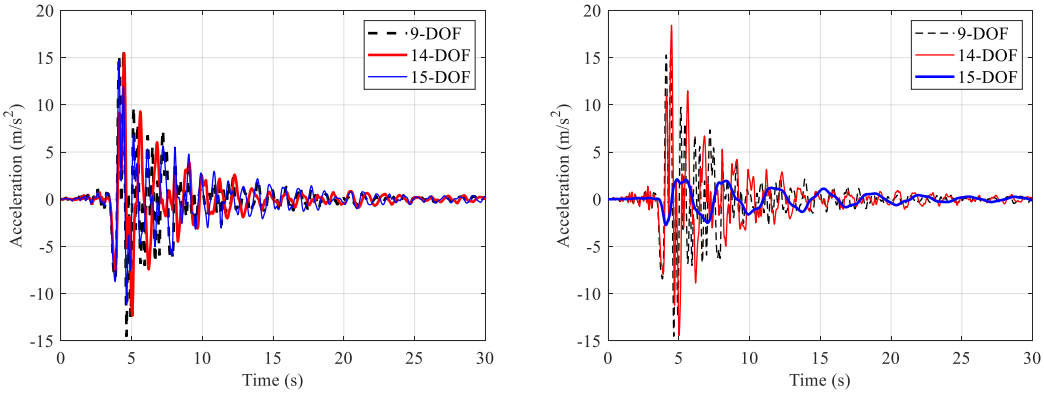

(a) (b)

Figure 4.2 Absolute Acceleration Comparison of (a) 9^{th} Floor (b) Top Floor

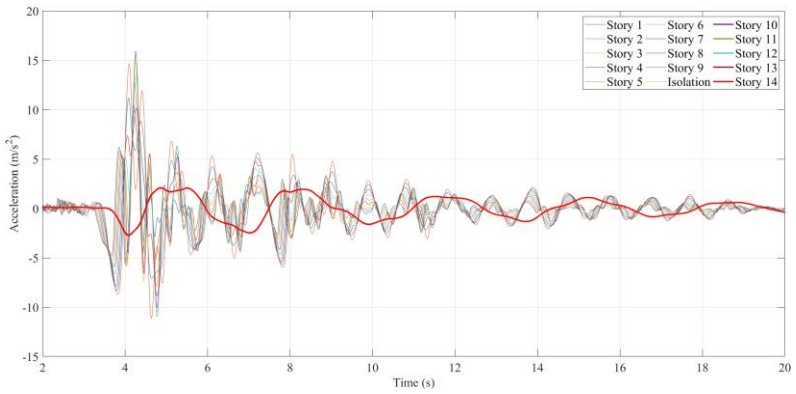

Figure 4.3 Acceleration of All Stories – Inter-story Isolated Structure

Table 4.1 Peak Response – (a) Kobe (b) El Centro (c) Northridge

(a)

Model	Base Shear (10^3 kN)	9th Floor Acceleration (m/s^2)	14th Floor Acceleration (m/s^2)	Inter-Story Isolation Drift (m)
9-DOF	619.5	24.42	-	-
14-DOF	489.3	13.66	16.13	-
15-DOF	638.0	23.72	2.42	0.637

(b)

Model	Base Shear (10^3 kN)	9th Floor Acceleration (m/s^2)	14th Floor Acceleration (m/s^2)	Inter-Story Isolation Drift (m)
9-DOF	243.2	8.06	-	-
14-DOF	190.4	4.55	18.42	-
15-DOF	251.3	8.68	1.19	0.310

(c)

Model	Base Shear (10^3 kN)	9th Floor Acceleration (m/s^2)	14th Floor Acceleration (m/s^2)	Inter-Story Isolation Drift (m)
9-DOF	562.2	15.78	-	-
14-DOF	647.4	15.47	18.42	-
15-DOF	489.6	14.68	2.73	0.726

While the reduced stiffness of the isolation layer allows for a reduction in the acceleration of the superstructure, it leads to large displacements in the isolation layer itself. Based on the displacement response for each ground motion, further displacement reduction is necessary to avoid damaging the isolators under larger magnitude earthquakes (Figure 4.4(a), Figure 4.4(c)). By adding damping to the isolation layer, the system will be able to dissipate more energy, thereby reducing the displacement of the isolation layer. Another means of adjusting the displacement response is to change the stiffness of the isolation layer. Both alternatives are assessed in Chapter 5.

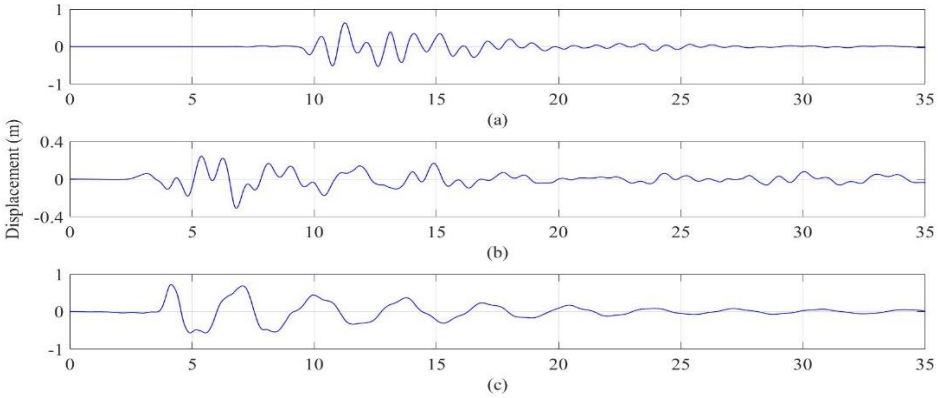

Figure 4.4 Isolation Layer Relative Displacement versus Time When Subject to Earthquake Ground Motion (a) Kobe (b) El Centro (c) Northridge

Figure 4.5 displays the fundamental frequency of each structure along with the frequency content of each ground motion. The standard retrofit lowers the fundamental natural frequency of the structure compared to the original structure, shifting it further from the dominant frequency content of the Kobe and El Centro ground motions. For the Northridge record, the frequency shift from standard retrofit leads to an overlap in frequency content and large base shear. In the case of the Northridge ground motion, inter-story isolation showed significant improvement in

base shear when compared to the other two structures (Table 4.1). For all other earthquakes, the base shear is comparable to the original structure.

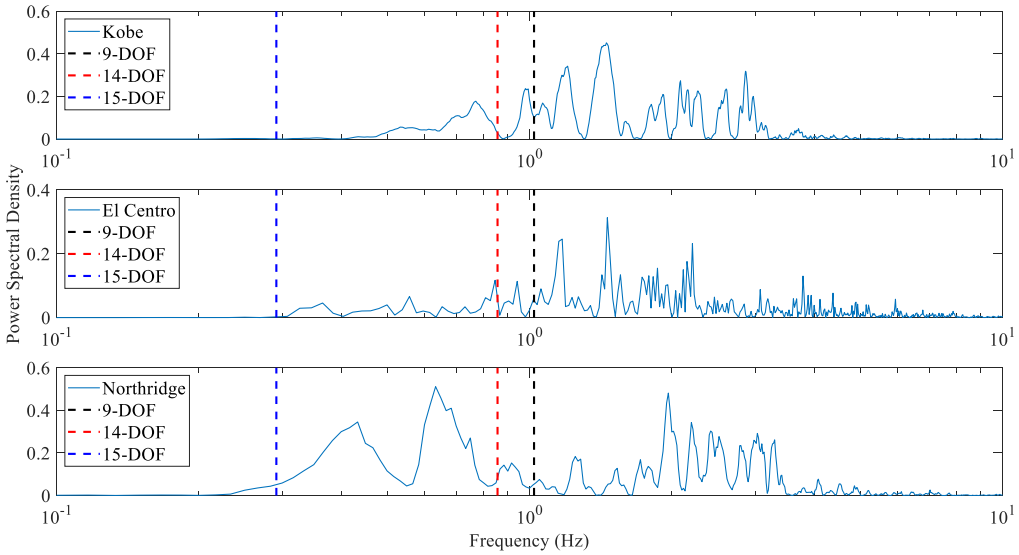

Figure 4.5 Frequency Content of Earthquake Ground Motion

4.3 Wind Load Analysis

An important design consideration for wind-induced vibration is the peak acceleration of each floor. This serviceability constraint impacts occupant comfort and well-being. The range of floor accelerations are presented in Table 4.2. The majority of occupants cannot perceive a floor acceleration below approximately 5 cm/s, or 0.5% of *g* (Zhou et al. 2003). An intolerable level of acceleration is considered to be greater than or equal to 150 cm/s.

Table 4.2 (adapted from Zhou et al. 2003)

Peak Acceleration (cm/s^2)	**Comfort Limit**
Less than 5	Not Perceptible
5 to 15	Threshold of Perceptibility
15 to 50	Annoying
50 to 150	Very Annoying
Greater than 150	Intolerable

Through a study on motion perception, Burton et al. attempted to relate these values to common experiences occupants may have at each acceleration (Burton et al. 2015). For example, the well-being limit for most occupants was found to be 10 cm/s, after which some occupants may become uncomfortable if such motion persists. An acceleration of about 40 cm/s, which generally only occurs under extreme wind events, causes fear in occupants and some may lose their balance. These constraints will give context for the values of acceleration of attained from the wind load analysis. The results of the analysis are tabulated in Table 4.3. A 60-second sample of the 42-minute time history responses of each structure are shown in Figures 4.6-4.7.

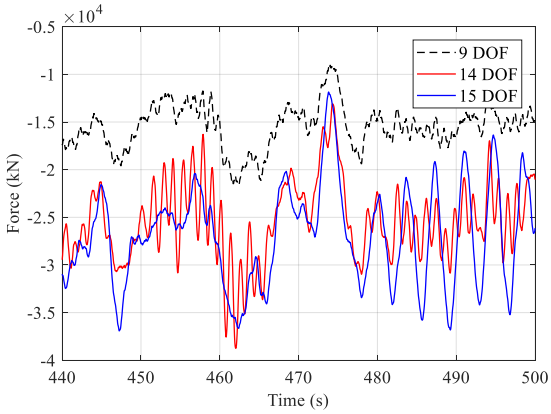

Figure 4.6 Base Shear

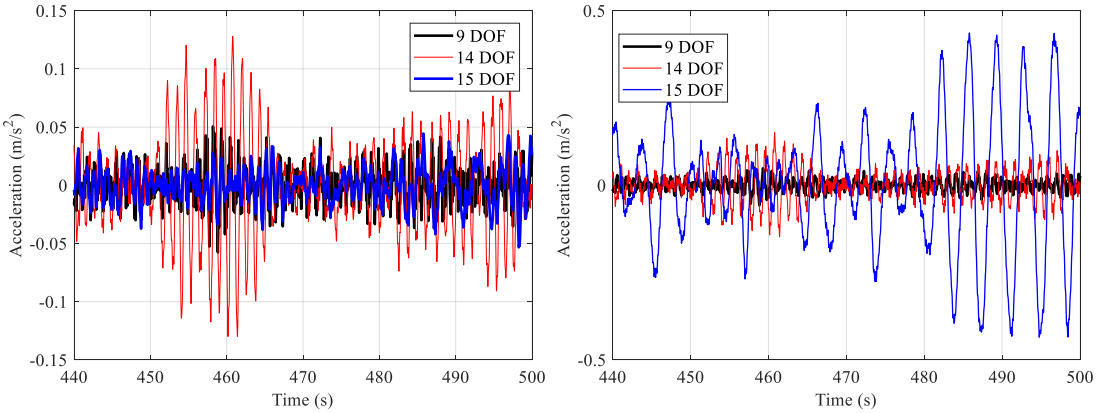

(a) (b)

Figure 4.7 Absolute Acceleration (a) 9th Floor (b) Top Floor

Table 4.3 Peak Response – Wind Load

Model	Base Shear (10^3 kN)	9th Floor Acceleration (cm/s^2)	14th Floor Acceleration (cm/s^2)	Inter-Story Isolation drift (m)
9-DOF	24.03	1.20	-	-
14-DOF	39.76	9.89	11.32	-
15-DOF	43.78	5.44	56.63	0.637

The 14-DOF and 15-DOF both have similar base shear demands that are higher than the original 9-DOF structure. By increasing the height of the 9-DOF structure, the total surface area subject to wind increased, which in turn increased the base shear on the structure.

The 9th floor acceleration for the 15-DOF structure is at the lower limit of human perceptibility, while the 14-DOF structure is on the higher end of the range of perceptibility. Building occupants on the 9th floor may find building motion more noticeable after a standard retrofit than after an inter-story isolation retrofit. However, for the standard retrofit, the acceleration at the top floor would be comparable to that of the 9th floor. Occupants would notice building motion but it would not significantly impede on their tasks unless such accelerations persisted. On the other hand, for an inter-story isolated retrofit, occupants of the floors above the isolation layer would experience large accelerations under severe wind loads which may incite fear and extreme discomfort. The large accelerations in the superstructure are low-frequency accelerations caused by the low stiffness in the isolation layer, which could be improved through the supplemental control methods of damping or increased isolation layer stiffness.

4.4 Summary

Both inter-story isolation and standard retrofit have benefits when performance is analyzed under excitation from the earthquakes studied. Inter-story isolation nominally decouples the substructure and superstructure, leading to low base shears and low accelerations in the superstructure. Standard retrofit lowers the overall fundamental natural frequency of the total structure. This leads to lower base shear and lower accelerations. The actual performance depends on the frequency content of the earthquake.

The effects of increased base shear on the foundation due to extreme winds may control more than earthquake ground motion for inter-story isolated buildings. This is due to the increase surface area that is subject to wind. However, for this particular structure, earthquake-induced base shears were an order of magnitude larger than the wind-induced base shears, negating this concern.

Also, the large reduction of top floor acceleration during a seismic event between a standard retrofit and inter-story isolated retrofit is a great benefit for the occupants of the floors above the isolation layer. However, the acceleration of the top floor may increase significantly under a wind when compared to conventional retrofit. It is worth noting there is an order of magnitude difference in accelerations between earthquake and wind. The earthquake induced-accelerations can cause damage, whereas the wind-induced accelerations are more of an occupant comfort concern.

For both earthquake and wind events, the ability of the installed isolators to handle these events should be confirmed. An important isolator design check is to confirm that the maximum isolator displacement does not cause the isolation system

to collapse (Feng et al. 2012). The maximum isolator displacement used by Murakami et al., where the parameters for the models originated, was about 40 cm, or half of the 80 cm isolator diameter (Murakami et al. 2008). This avoids the potential of creating overturning moments within the isolators. The maximum isolator displacement for the earthquake and wind analysis were 0.726 m and 0.637 m, respectively. For the wind load, this changes the concerns for serviceability and occupant comfort into a structural concern. To reduce this displacement, improvements should be made to the isolation layer.

Chapter 5: Improvements to Inter-Story Isolation

5.1 Overview

5.1.1 Supplemental Damping

To further improve the performance of the inter-story isolation system, damping may be added to the structure. Increased damping will decrease displacement of the isolation layer, but can negate some of the benefits of isolation such as reduced superstructure acceleration. The two damping models explored in this paper are viscous damping and rate-independent linear damping (RILD). Viscous damping and RILD were each added to the structure in the form of discrete damping at the isolation layer. Both damping methods were analyzed to observe how they affected the dynamic behavior of the structure.

For simplicity, a viscous damping coefficient was calculated based on the target criteria in Chapter 5.2 and the total viscous damping force was applied to the model by adding the damping coefficient to the 10th DOF (inter-story isolation layer) damping coefficient (Table 3-1c). Equation 5-1 describes the viscous damping force in terms of time *t*, the viscous damping coefficient $c_{viscous}$, and the relative velocity between the 9th and 10th DOF $\dot{x}(t)$.

$$f_v(t) = c_{viscous} * \dot{x}(t) \qquad (5\text{-}1)$$

Viscous dampers are commonly-used devices and have a cap on the maximum force, which is unaccounted for in these simulations. A set of dampers can be installed at the isolation layer to provide the total viscous damping force necessary to adequately reduce the response of the building per design codes. On the other hand,

the implementation of RILD is more difficult to achieve. RILD is non-causal, in that its response cannot be calculated in a standard time history analysis. Equation 5-2 represents the RILD force in the time domain while equation 5-3 represents RILD in the frequency domain (Inaudi and Kelly 1995) in terms of isolation layer stiffness *k*, the ratio between the loss modulus and storage modulus η, imaginary unit *i*, signum function *sign( )*, and Hilbert transform $\hat{x}(t)$. The Hilbert transform can also be expressed using the Cauchy principal value *p.v.* (Equation 5-4).

$$f_D(t) = k\eta\hat{x}(t) \tag{5-2}$$

$$F_D(\omega) = \eta k i sign(\omega) x(\omega) \tag{5-3}$$

$$\hat{x}(t) = \frac{1}{\pi} p.v. \int_{-\infty}^{\infty} \frac{x(t)}{t-\tau} d\tau \tag{5-4}$$

The parameter η is used to adjust the damping in the structure. The damping coefficient ($k\eta$) was added to the isolation layer as a discrete damping source. This method was evaluated in the frequency domain because the damping force is calculated using the displacement response which has been advanced in phase $\pi/2$ radians.

5.1.2 Varying Isolation Layer Stiffness

Different dynamic behaviors can also be created in the structure by varying the stiffness of the isolation layer. Equation 3-1 shows that the natural frequencies of the structure are dependent on both the mass and stiffness matrices. Increasing the stiffness so that the super structure and substructure have the same fundamental frequency causes the superstructure to act as a tuned mass damper (TMD) for the

substructure. Increasing the stiffness further results in dynamic behavior similar to that of a standard structure.

To compare the effects of different stiffness values on the structural behavior, three scenarios were considered (low, intermediate, and high stiffness) and subject to the Northridge earthquake ground motion. The three cases are defined by the following ratio, *R*, where ω_{sup} is the first natural frequency of the superstructure and ω_{sub} is the first natural frequency of the substructure.

$$R = \frac{\omega_{sup}}{\omega_{sub}} \tag{5-5}$$

5.2 Earthquake

5.2.1 Supplemental Damping

The viscous damping and RILD coefficients were both calibrated in order to meet the following target criteria. The largest displacement response occurred with the Northridge earthquake; therefore, the selected target criteria of each damping method was to reduce the peak displacement of the isolation layer by approximately 20% when excited by the Northridge ground motion. This resulted in a viscous damping coefficient $c_{viscous}$ of $1.172*10^7$, and η of 0.638. The resulting performance is depicted in Figure 5.1 and peak responses presented in Table 5.1.

Table 5.1 Peak Response (a) Kobe (b) El Centro (c) Northridge

(a)

Damping Type	Isolation Layer Relative Displacement (m)	Base Shear (10^3 kN)	9th Floor Acceleration (m/s^2)	14th Floor Acceleration (m/s^2)	Damping Force (10^3 kN)
None	0.637	637.95	23.72	2.42	-
Viscous	0.495	552.09	20.09	3.46	35.14
RILD	0.533	600.09	21.70	2.79	19.02

(b)

Damping Type	Isolation Layer Relative Displacement (m)	Base Shear (10^3 kN)	9th Floor Acceleration (m/s^2)	14th Floor Acceleration (m/s^2)	Damping Force (10^3 kN)
None	0.310	251.27	8.68	1.19	-
Viscous	0.221	199.34	6.35	1.50	12.39
RILD	0.238	227.27	7.48	1.25	7.67

(c)

Damping Type	Isolation Layer Relative Displacement (m)	Base Shear (10^3 kN)	9th Floor Acceleration (m/s^2)	14th Floor Acceleration (m/s^2)	Damping Force (10^3 kN)
None	0.726	489.49	14.68	2.73	-
Viscous	0.592	466.65	13.48	3.53	32.31
RILD	0.592	490.12	14.15	2.68	22.86

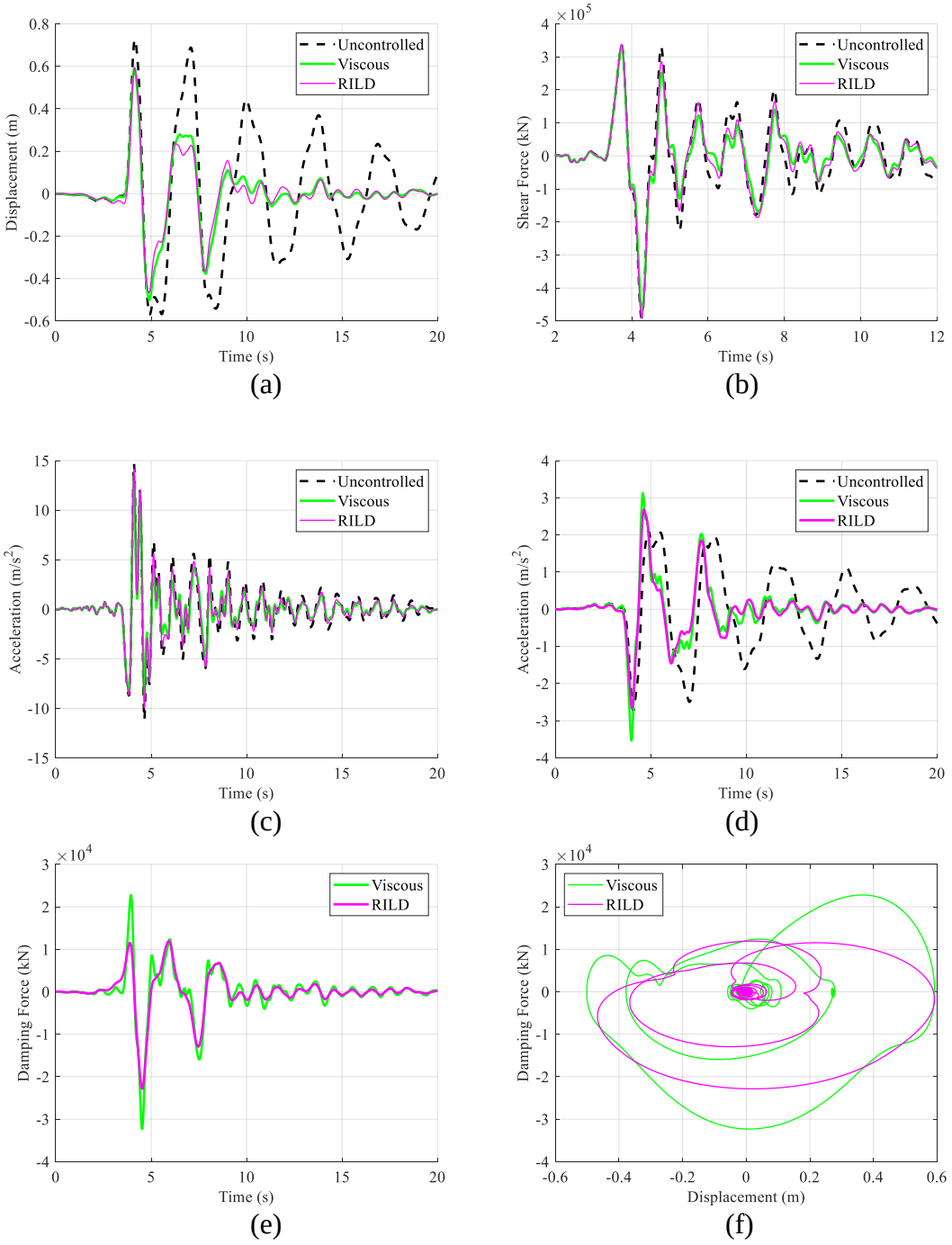

Figure 5.1 Damping Performance Comparison for Northridge Earthquake (a) Inter-story Drift of Isolation Layer (b) Base Shear (c) Absolute Acceleration of 9th Floor (d) Absolute Acceleration of Top Floor (e) Damping Force (f) Damping Force Hysteresis

Due to the trade-off that exists between displacement and acceleration, most supplemental damping cases decreased the isolation layer displacement at the expense

of increasing the top floor acceleration. The peak acceleration of the top floor of the building for the RILD case, however, was 17-24% lower than the peak acceleration response for the viscous case. Additionally, the damping force for the RILD case was 30-45% lower than the viscous case. The lower accelerations will decrease discomfort experienced by the building occupants. RILD produces a more efficient damping method for inter-story isolation because it can reduce accelerations above the isolation with a lower damping force.

In addition to reducing displacement, additional damping generally decreased the base shear for each earthquake. More damping means more energy is dissipated at the isolation layer, reducing the overall force on the base of the structure. This is also an indication that adding additional damping to the isolation layer will not put any additional stress on the foundation of the building.

5.2.2 Varying Isolation Layer Stiffness

The initial value of *R* for the given structural parameters of the inter-story isolated structure is 0.29. A value of 1.0 represents a TMD, while a higher value of about 3.0 produces un-isolated behavior. All models have the consistent Rayleigh damping of 5% and 4% for the first and second modes, respectively. The results of the analysis are expressed in Figure 5.2.

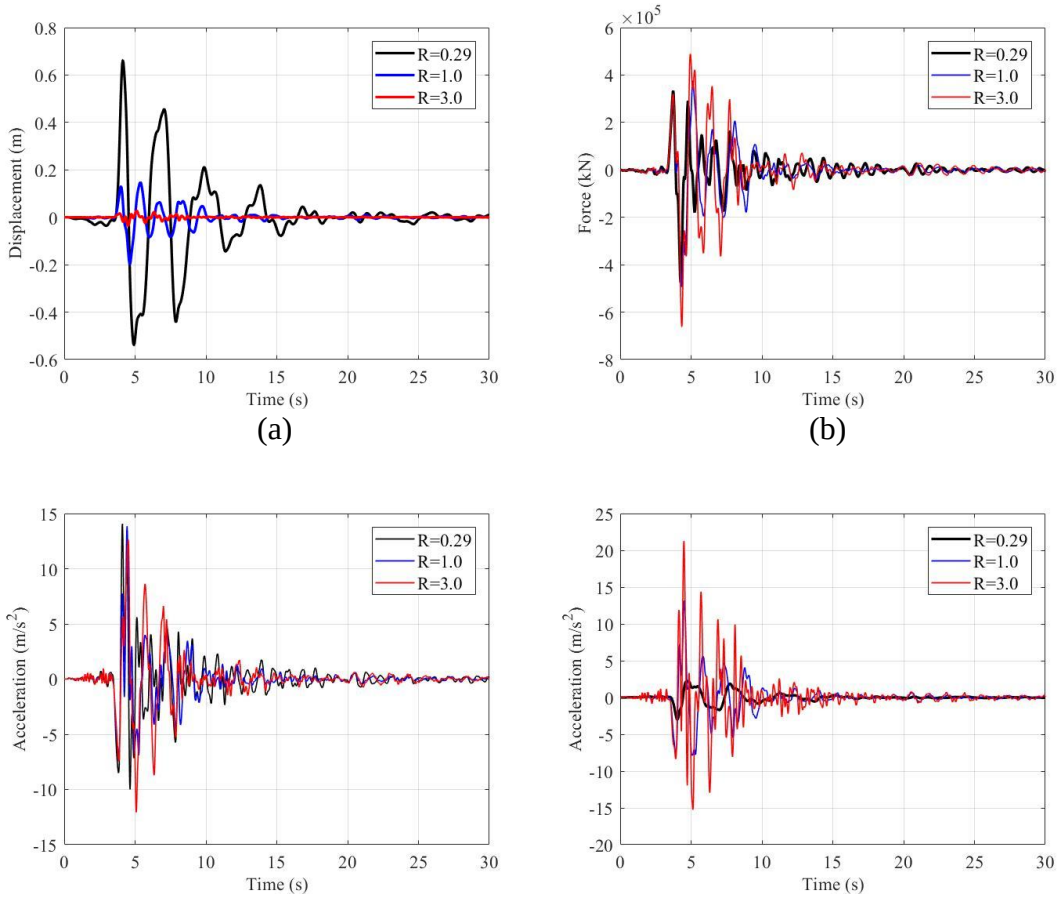

Figure 5.2 Stiffness Performance Comparison for Northridge Earthquake (a) Inter-story Drift of Isolation Layer (b) Base Shear (c) Absolute Acceleration of the 9th Floor (d) Absolute Acceleration of the Top Floor

Table 5.2 Peak Response for Varied Stiffness (a) Kobe (b) El Centro (c) Northridge

(a)

Stiffness Ratio (R)	Isolation Layer Relative Displacement (m)	Base Shear (10^3 kN)	9th Floor Acceleration (m/s^2)	14th Floor Acceleration (m/s^2)
0.29	0.5684	598.3	21.66	2.70
1.0	0.1619	365.4	12.04	11.97
3.0	0.0296	602.5	11.38	17.02

(b)

Stiffness Ratio (R)	Isolation Layer Relative Displacement (m)	Base Shear (10^3 kN)	9th Floor Acceleration (m/s^2)	14th Floor Acceleration (m/s^2)
0.29	0.2680	226.2	7.55	1.30
1.0	0.0441	98.3	3.11	2.89
3.0	0.0082	193.2	3.95	5.43

(c)

Stiffness Ratio (R)	Isolation Layer Relative Displacement (m)	Base Shear (10^3 kN)	9th Floor Acceleration (m/s^2)	14th Floor Acceleration (m/s^2)
0.29	0.6619	476.3	14.07	3.01
1.0	0.1978	493.4	13.85	13.17
3.0	0.0363	662.0	12.62	21.26

As expected, the inter-story displacement at the isolation layer decreased as the stiffness of the isolation layer increased. Additionally, the acceleration of the floors above the isolation layer increased as the stiffness of the isolation layer increased. Especially for the TMD case where R=1.0, the superstructure should resonate at the same natural frequency as the substructure, thus dissipating energy and reducing the peak accelerations of the substructure. When excited by the Northridge earthquake, the acceleration of the 9th floor decreased slightly from 14.07 to 13.85 (1.5%) when R=1.0 and from 14.07 to 12.62 (10%) for R=3.0. The low stiffness and TMD cases are comparable enough that the effectiveness of the system against wind forces will determine whether or not the difference in peak acceleration due to

earthquake ground motion is a reasonable trade-off in order to further reduce the wind vibration response.

Using a consistent damping ratio of 5% for the first mode and 4% for the second mode and discretizing the range of stiffness values further results in the following relationships depicted in Figures 5.3-5.4. For *R* values less than 1, the superstructure acceleration increased significantly as the substructure acceleration generally decreased (Figure 5.4).

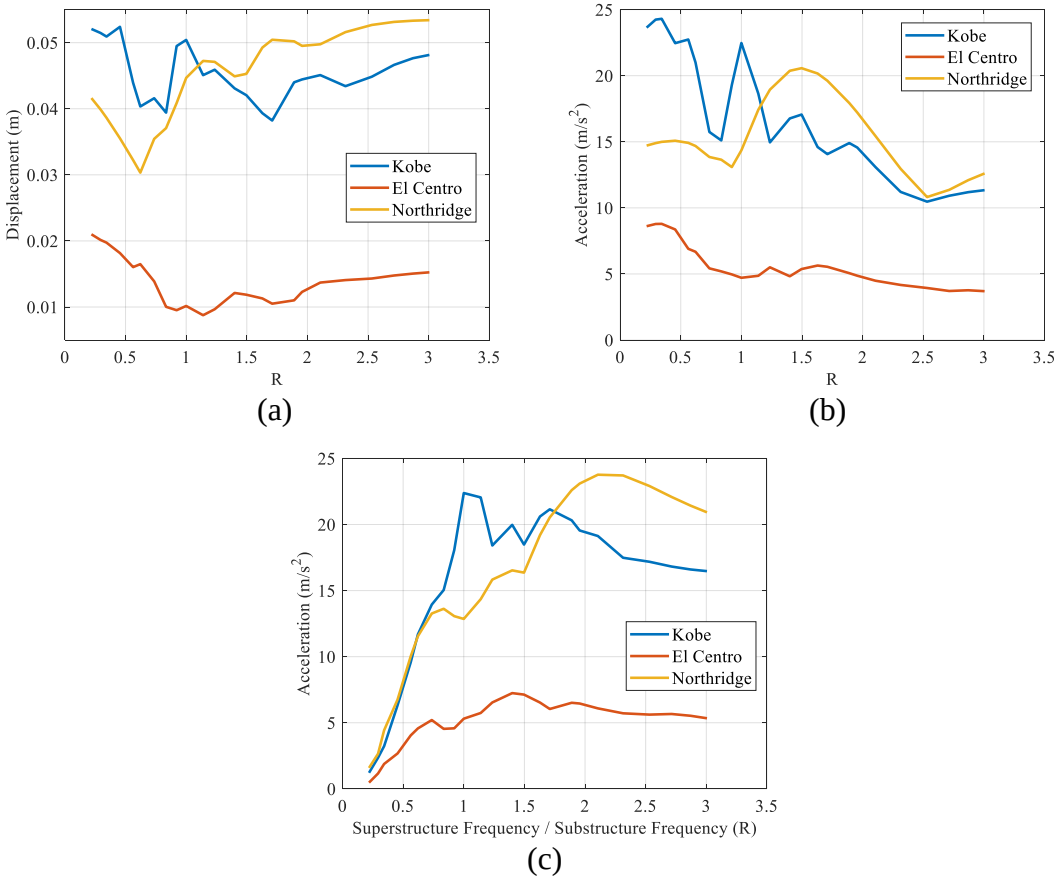

Figure 5.3 Peak Response vs Stiffness (a) First Floor Displacement (b) 9th Floor Acceleration (c) Top Floor Acceleration

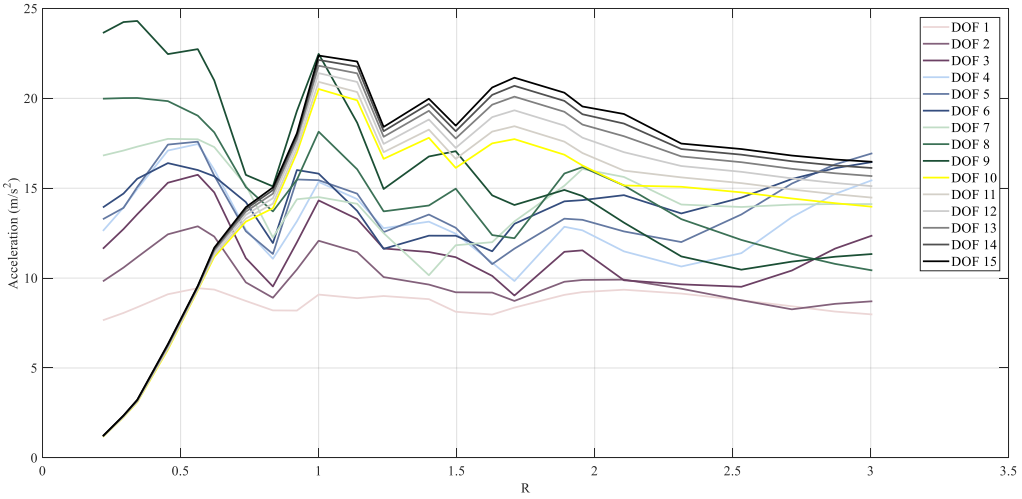

Figure 5.4 Peak Acceleration Response vs Stiffness for Kobe Earthquake

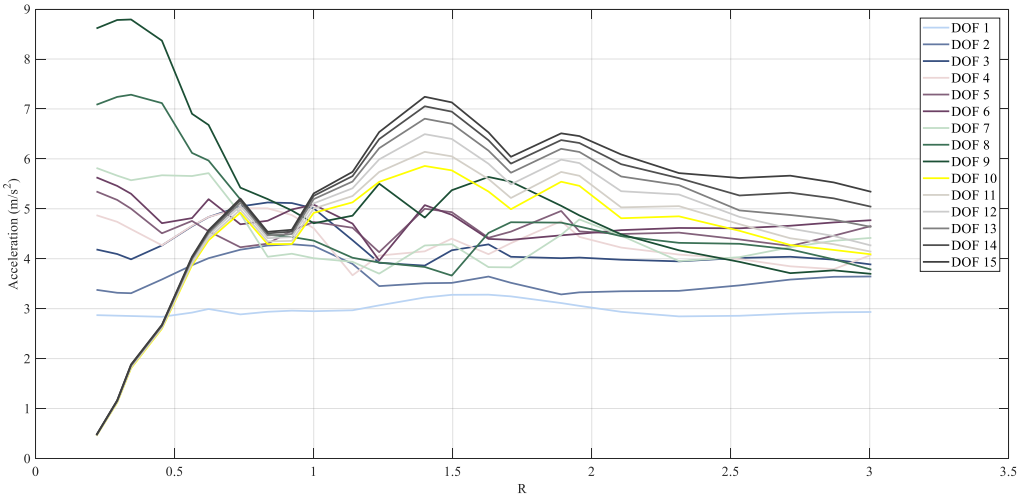

Figure 5.5 Peak Acceleration Response vs Stiffness for El Centro Earthquake

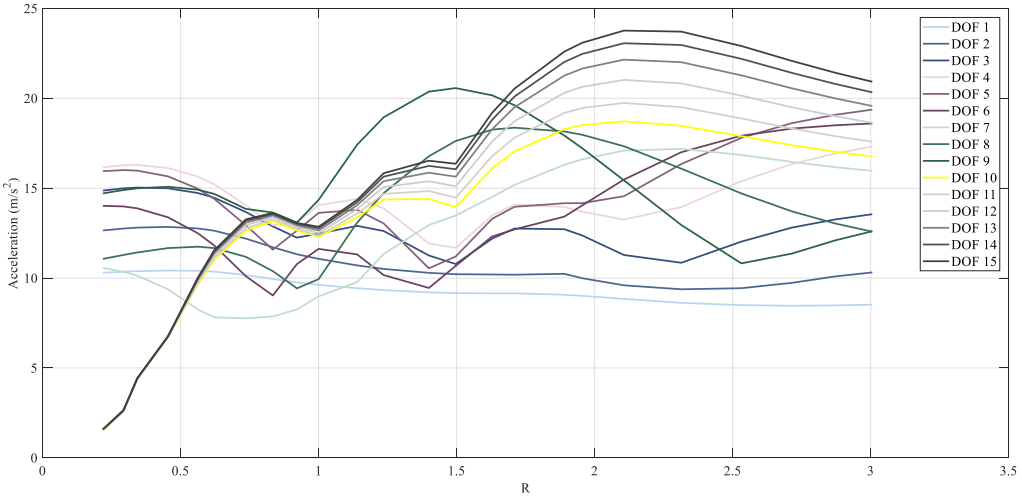

Figure 5.6 Peak Acceleration Response vs Stiffness for Northridge Earthquake

The results of discretization are inconclusive. The peak response of the structure does indeed vary with stiffness, but it is also clear that both the magnitude and frequency content of the input ground motion greatly influences the trend of the peak response versus *R*. To investigate further, adequate damping should be applied to the TMD case.

5.2.3 Supplemental Damping for TMD

As alluded to in the previous section, a TMD has an optimal damping ratio which generally requires up to 20% damping in order to be an effective protective system. By increasing the isolation layer stiffness to a ratio of *R*=1.0 and adding viscous damping and RILD, the combined benefits of the TMD and supplemental damping can be realized. The target criteria for this case is to reduce the maximum inter-story displacement by 30%. In the TMD case, the maximum displacement occurs with the Kobe earthquake ground motion; therefore, the viscous and RILD parameters were designed to reduce the inter-story displacement response to the Kobe earthquake by 30%. The analysis results are presented in Table 5.3 and Figures 5.7a-5.7f.

Table 5.3 TMD Peak Response (a) Kobe (b) El Centro (c) Northridge (a)

Damping Type	Isolation Layer Relative Displacement (m)	Base Shear (10^3 kN)	9th Floor Acceleration (m/s^2)	14th Floor Acceleration (m/s^2)	Damping Force (10^3 kN)
None	0.5016	617.05	22.29	22.27	-
Viscous	0.3511	403.65	15.22	15.92	38.46
RILD	0.3511	408.85	16.25	15.85	36.43

(b)

Damping Type	Isolation Layer Relative Displacement (m)	Base Shear (10^3 kN)	9th Floor Acceleration (m/s^2)	14th Floor Acceleration (m/s^2)	Damping Force (10^3 kN)
None	0.1191	124.46	4.70	5.28	-
Viscous	0.0837	99.41	4.09	3.78	13.90
RILD	0.0860	103.83	4.41	3.98	11.18

(c)

Damping Type	Isolation Layer Relative Displacement (m)	Base Shear (10^3 kN)	9th Floor Acceleration (m/s^2)	14th Floor Acceleration (m/s^2)	Damping Force (10^3 kN)
None	0.2987	549.63	14.38	12.87	-
Viscous	0.2609	477.67	14.41	11.50	35.06
RILD	0.2491	485.94	14.68	10.64	35.28

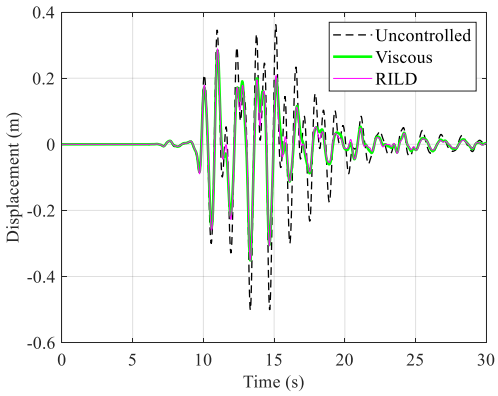

(a)

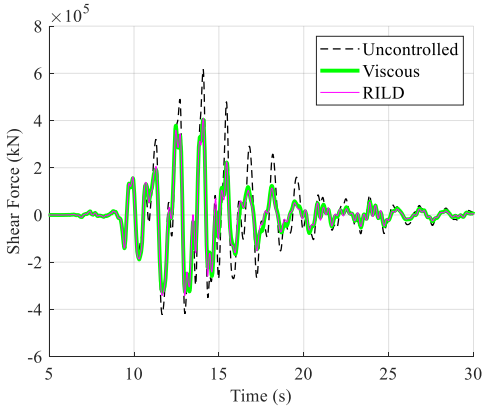

(b)

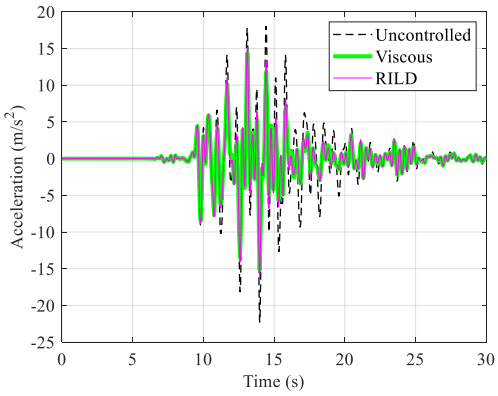

(c)

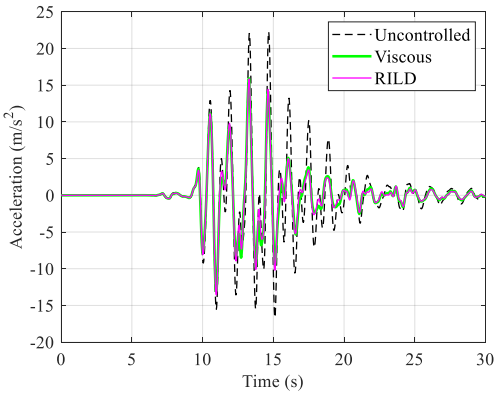

(d)

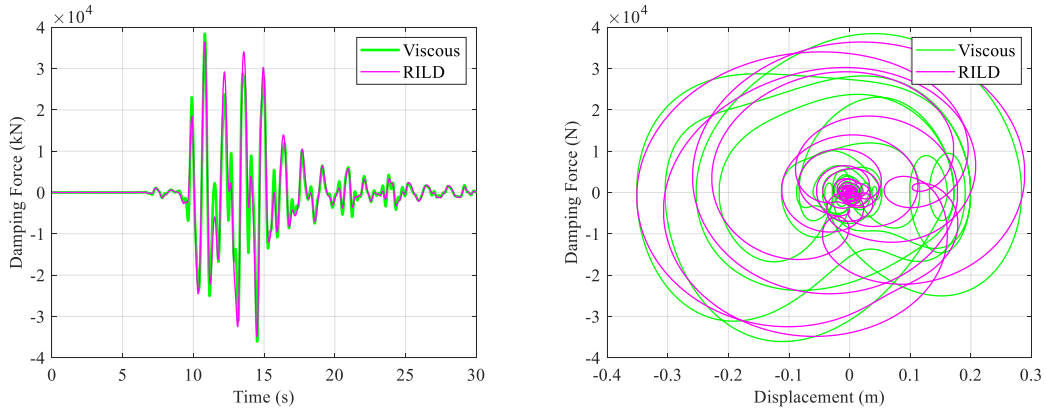

Figure 5.7 TMD Damping Performance Comparison for Northridge (a) Inter-story Drift of Isolation Layer (b) Base Shear (c) Absolute Acceleration of 9th Floor (d) Absolute Acceleration of Top Floor (e) Damping Force (f) Damping Force Hysteresis

In certain situations similar to the Kobe earthquake, adding damping to the TMD case may reduce the acceleration of the substructure up to about 30%. In others more similar to El Centro or Northridge, the acceleration of the substructure is reduced slightly, but overall is comparable. For the low-stiffness isolation layer, reducing the displacement response generally yields an increase to the superstructure acceleration for both viscous and RILD (Table 5.1), but at the cost of increasing the superstructure acceleration. Adding damping after increasing the stiffness so that the superstructure acts as a TMD was also found to reduce the acceleration response of the superstructure. As seen in tables 5.3a and 5.3b, the 9th floor and 14th floor accelerations are very close. Additionally, for Tables 5.3b, the acceleration of the superstructure was actually less than that of the substructure. This behavior does not reflect a conventional inter-story isolation system, as the superstructure accelerations are much higher than presented in Tables 4.3 and 5.1, but may provide an alternative approach to modifying inter-story isolation to use as a multi-hazard protective system.

5.3 Wind

5.3.1 Supplemental Damping

Because inter-story isolation is a protective system primarily designed for seismic excitation, the priority for design of the damping parameters was given to earthquake protection. The following building performance under an extreme wind event uses the damping parameters that were determined in Chapter 5.2.1. The analysis results are presented in Table 5.4. Note that the values presented are not true peaks, but peaks estimated using extreme value analysis as described in Section 3.5.

Table 5.4 Peak Response with Damping

Damping Type	Isolation Layer Relative Displacement (m)	Base Shear (10^3 kN)	9th Floor Acceleration (cm/s^2)	14th Floor Acceleration (cm/s^2)	Damping Force (10^3 kN)
None	0.4383	43.78	5.44	56.63	-
Viscous	0.3630	40.86	4.17	26.84	1.68
RILD	0.2660	40.44	5.60	23.70	4.65

Both damping methods reduce the isolation layer displacement, viscous by 17% and RILD by 39%, which bring both displacements to be less than half of the 80-cm isolator diameter. The base shear also decreased by about 7%, slightly reducing the stress on the foundation. Viscous damping and RILD also reduced the top floor acceleration by 53% and 58%, respectively without significantly increasing the acceleration of the substructure. This confirms that supplemental damping allows more energy to be dissipated at the isolation layer. RILD produces a larger damping force than viscous damping, but both are still much smaller when compared to the maximum damping force produces under earthquake excitation (see Table 5.1).

5.3.2 Varying Stiffness of Isolation Layer

The results of using low, intermediate, and high stiffness cases are presented in Table 5.5. The ratio R=1.0 is representative of the superstructure acting as a TMD for the substructure. All models have the consistent Rayleigh damping of 5% and 4% for the first and second modes, respectively.

Table 5.5 Peak Response with Varied Stiffness

Stiffness Ratio (R)	Isolation Layer Relative Displacement (m)	Base Shear (10^3 kN)	9^{th} Floor Acceleration (cm/s^2)	14^{th} Floor Acceleration (cm/s^2)
0.29	0.4448	44.88	5.60	56.14
1.0	0.0322	44.51	12.72	22.98
3.0	0.0025	43.38	10.95	13.31

The results show that the 9^{th} floor acceleration, below the isolation layer, does increase with stiffness to a point (Figure 5.9). The increase is slight and may be noticeable due to the fact that the TMD and high stiffness cases are within the threshold of human perceptibility (see Table 4.2). Conversely, the maximum acceleration of the superstructure produced with the low-stiffness case is in the range of "Very Annoying" motion and may cause building occupants to be alarmed, while the TMD case reduces the acceleration to "Annoying" and the higher stiffness case further reduces the acceleration to the range of possible human perception. With a low isolator stiffness, the superstructure is imitating base isolation behavior, which has been found to perform poorly under wind excitation (Anajafi and Medina 2017). By increasing the stiffness to create a TMD, the structural behavior changes and more energy remains in the substructure, subsequently reducing the superstructure acceleration. This distinction would have greater impacts on the well-being and safety

of building occupants in the superstructure the longer than such accelerations persist. Additionally, the relative displacement of the TMD case is approximately 7% of the low-stiffness case. The displacement for the low stiffness case is already about half of the 80 cm diameter of the rubber isolators currently installed. The amount of wear on the isolators will be much less with lower displacements, and displacements greater than 40 cm can damage them.

Discretizing the values of *R* further, each peak response of the structure can be plotted against its frequency ratio *R*. For example, the peak displacement of the first floor (Figure 5.8a), the peak acceleration of the 9th floor (Figure 5.8b), and the peak acceleration of the top floor (Figure 5.8c) plotted versus *R*.

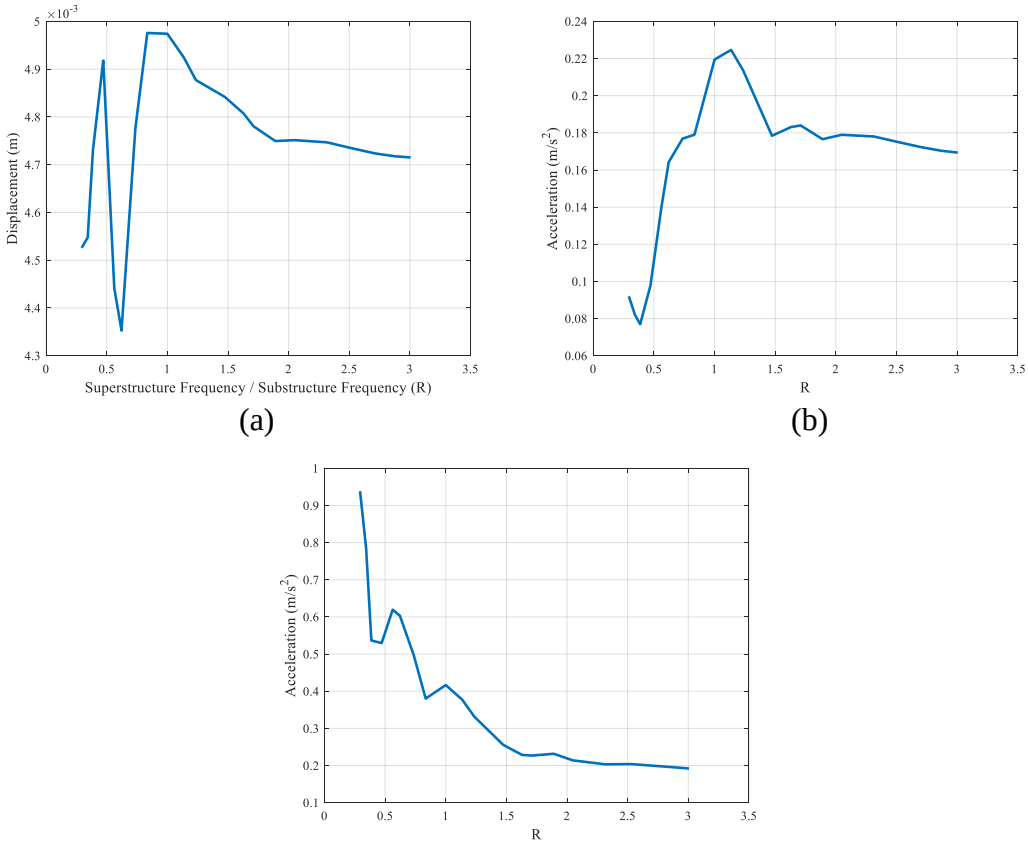

(a) (b)

(c)

Figure 5.8 Peak Wind Response vs R (a) First Floor Displacement (b) 9th Floor Acceleration (c) Top Floor Acceleration

It is apparent from Figure 5.8 that as the stiffness increases, the acceleration of the substructure increases and the acceleration of the superstructure decreases. As far as occupant well-being, those on the substructure floors would experience unimposing vibrations for *R* less than 0.5 (Table 4.2). The maximum appears to occur when *R* is equal to about 1-1.2. These values then decrease and remain constant at an *R* of about 2.5. The superstructure acceleration decreases significantly from R=0.29 to R=1.0. The acceleration of the superstructure in this range, without any inherent damping, is dangerous and extremely disruptive for occupants. Increasing the stiffness reduces the acceleration by reducing the isolation behavior until the isolators act as a rigid connection between degrees of freedom 9 and 10.

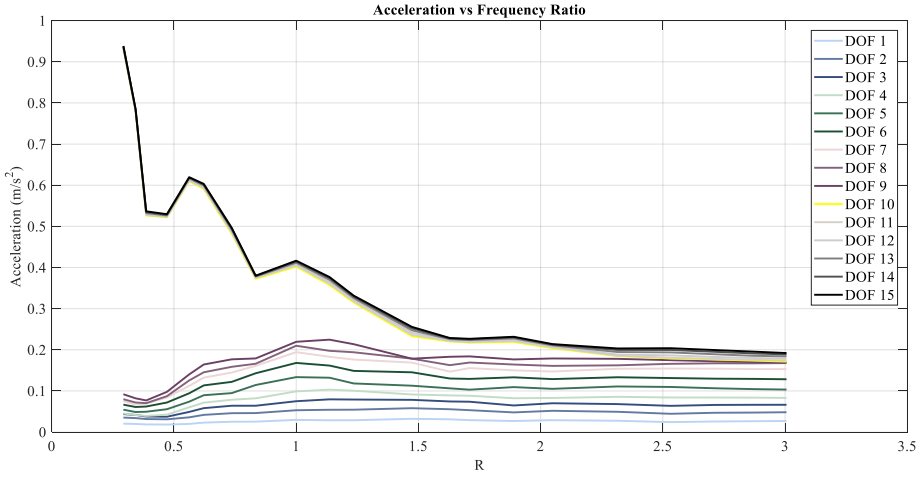

Figure 5.9 Peak Acceleration of each Degree of Freedom

5.3.3 Supplemental Damping for TMD

To better estimate the performance of the TMD, additional damping should be added. Tuned mass dampers generally require 10-20% damping in order to be effective. Therefore, supplemental discrete damping was added to the isolation layer so that a more effective TMD could be analyzed. The results in Table 5.6 are the

result of analyzing the structure with R=1.0 and damping coefficients determined from earthquake analysis in section 5.2.3. The isolation layer displacement is reduced and base shear is about the same when compared to the low-stiffness isolation case, (see Table 5.4). The damping force is also reduced by about 75%. However, the 9th floor acceleration is much higher than the low-stiffness analysis, making this system less effective at maintaining inter-story isolated behavior (Table 5.4).

Table 5.6 TMD Peak Response with Damping

Damping Type	Isolation Layer Relative Displacement (m)	Base Shear (10^3 kN)	9th Floor Acceleration (cm/s^2)	14th Floor Acceleration (cm/s^2)	Damping Force (10^3 kN)
None	0.0323	44.49	14.16	26.29	-
Viscous	0.0318	43.78	12.49	23.47	0.4421
RILD	0.0305	43.54	12.31	21.26	1.635

5.4 Summary

By introducing supplemental damping and an informed selection of the isolation layer stiffness, inter-story isolation performance can be further improved. The displacement of the isolation layer can be reduced effectively with supplemental damping, increased isolation stiffness, or a combination of the two. Base shear and floor accelerations are still much higher under earthquake excitation; accelerations are on the magnitude of m/s^2 as opposed to cm/s^2, which confirms that designing protection against earthquake should be prioritized. RILD outperformed viscous damping under earthquake loading, but created relatively large accelerations in the superstructure under wind loading. The option of adding supplemental damping after increasing the isolation stiffness and using the superstructure as a TMD does reduce isolation layer displacement, but at the expense of increasing the acceleration of the

substructure. Supplemental RILD produced promising results for improving the performance of the original, low-stiffness inter-story isolated structure under both earthquake and wind loads. In order to fully realize the benefits of RILD, a causal implementation must be explored.

Chapter 6: Practical Implementation of RILD

6.1 Overview

Practical implementations of viscous damping already exist. The focus of this section is to on RILD because practical application of it is uncommon. This provides motivation to realize non-causal RILD in a time-dependent manner. The causal force can then be realized through semi-active control. Another motivator is the fact that the RILD damping force is related to displacement. Viscous damping can be too low at low-frequencies, not sufficiently suppressing isolator displacement. Viscous damping can be too high at high-frequencies, leading to larger superstructure accelerations. RILD, on the other hand, is frequency independent, pairing well with the desired performance of isolated systems.

Inter-story isolated structures have a lower fundamental natural frequency than a conventionally constructed structure. The first mode shape produces large displacements concentrated at the isolation layer (Figure 3.6), which should allow for adequate damping to be produced using RILD. The purpose of investigating causal RILD is to reproduce this relationship and provide a promising robust damping method for inter-story isolated structures.

The causal implementation approximates the non-causal damping force of equation 6-1 using an all-pass filter (Keivan et al. 2017). Equation 6-2 represents the causal filer-based (CFB) approximation of the output damping force given a displacement input, where ω_o is the frequency where $H_{\mathrm{CFB}}(\omega)$ has a $\pi/2$ phase advance.

$$H_{RILD}(\omega) = \eta k i * sign(\omega) \tag{6-1}$$

$$H_{CFB}(\omega) = \eta k \frac{i\omega - \omega_o}{i\omega + \omega_o} \tag{6-2}$$

To have a reasonable causal replication of RILD for earthquake and wind loading, adjustments to the CFB model were made. Wind contains much more low-frequency input than earthquakes, so an additional step was taken to filter out a portion of the low-frequency input to the CFB model using a high-pass, second order Butterworth filter with a frequency of 0.31 rad/s (0.05 Hz). Additionally, the frequency ω_o was adjusted to compensate for the phase delay of the high-pass filter.

For earthquake analysis, using the natural frequency of the substructure for ω_o works well because the ground motion is filtered by the substructure and the response at the inter-story isolation layer is concentrated at the fundamental natural frequency of the substructure. For wind analysis, an adaptive controller was added so that the frequency of the CFB model coincides with the dominate response frequency of the structure as it changes over time. Implementing an adaptive controller automatically tunes the filter frequency to match the response frequency in a realistic scenario. One such algorithm proposed by Keivan et al., the Adaptive A-D controller, approximates the dominant natural frequency using the relative displacement and relative acceleration of the isolation layer (Keivan 2018). A linear-least-squares fit of the relative acceleration versus the relative displacement in Cartesian coordinates. The square root of the negative slope of the linear fit can be used as an approximation of the dominant response frequency. The approach is expressed in equation 6-3 at time t_i for response frequency ω_{fi}, where n is the number of samples and $\bar{x}$ and $\bar{\ddot{x}}$ are the

displacement and acceleration sample means, respectively. For this study, ω_{fi} was calculated and updated in the causal filter every 10 seconds.

$$\omega_{fi} = \sqrt{\frac{\sum_{j=i-n+1}^{i}(x_j - \bar{x})(\ddot{x}_j - \bar{\ddot{x}})}{\sum_{j=i-n+1}^{i}(x_j - \bar{x})^2}} \tag{6-3}$$

6.2 Earthquake

Due to the random nature of earthquake frequency and magnitude, it is unreasonable to design a protective system to mitigate the response of one specific earthquake record. Instead, a proactive approach is to implement a system that can reasonably reduce the response of the model under a variety of loading scenarios. In scenarios where the input excitation is about the same as the natural frequency of the structure, the contribution from the first mode will dominate the overall response (Chopra 2012). Because of these factors, the first natural frequency of the substructure, 6.42 rad/s (1.02 Hz) was selected for the transfer function frequency ω_o in equation 6-2. Viscous damping is also provided for a point of comparison. In order to meet the same target criteria for supplemental damping as in the previous chapter, 20% of the maximum displacement response, the viscous damping coefficient $c_{viscous}$ was set to $11.72*10^3$ kN*s/m, and the parameter η for non-causal and causal RILD was set to 0.638 and 1.0 respectively. The results for the Kobe earthquake input is shown in Figure 6.1a-6.1f. Results from all ground motions are expressed in Tables 6.1a-6.1c.

Table 6.1 Causal RILD Peak Response for Earthquake (a) Kobe (b) El Centro (c) Northridge

(a)

Case	Displacement of Isolation Layer (m)	Base Shear (10^3 kN)	9th Floor Acceleration (m/s^2)	14th Floor Acceleration (m/s^2)	Damping Force (10^3 kN)
Viscous	0.495	552.09	20.09	3.46	35.14
Non-causal	0.533	600.09	21.71	2.79	19.02
Causal Filter-Based	0.504	590.41	21.39	3.01	27.36
% Difference from Non-causal	5.44%	1.61%	1.47%	7.89%	43.85%

(b)

Case	Displacement of Isolation Layer (m)	Base Shear (10^3 kN)	9th Floor Acceleration (m/s^2)	14th Floor Acceleration (m/s^2)	Damping Force (10^3 kN)
Viscous	0.221	199.34	6.35	1.50	12.39
Non-causal	0.238	227.27	7.48	1.25	7.66
Causal Filter-Based	0.185	214.31	7.07	1.11	8.80
% Difference from Non-causal	22.27%	5.07%	5.48%	11.2%	14.88%

(c)

Case	Displacement of Isolation Layer (m)	Base Shear (10^3 kN)	9th Floor Acceleration (m/s^2)	14th Floor Acceleration (m/s^2)	Damping Force (10^3 kN)
Viscous	0.592	466.65	13.48	3.53	32.31
Non-causal	0.592	490.12	14.15	2.68	22.86
Causal Filter-Based	0.592	496.43	14.17	2.46	31.12
% Difference from Non-causal	0%	1.29%	0.141%	8.21%	36.12%

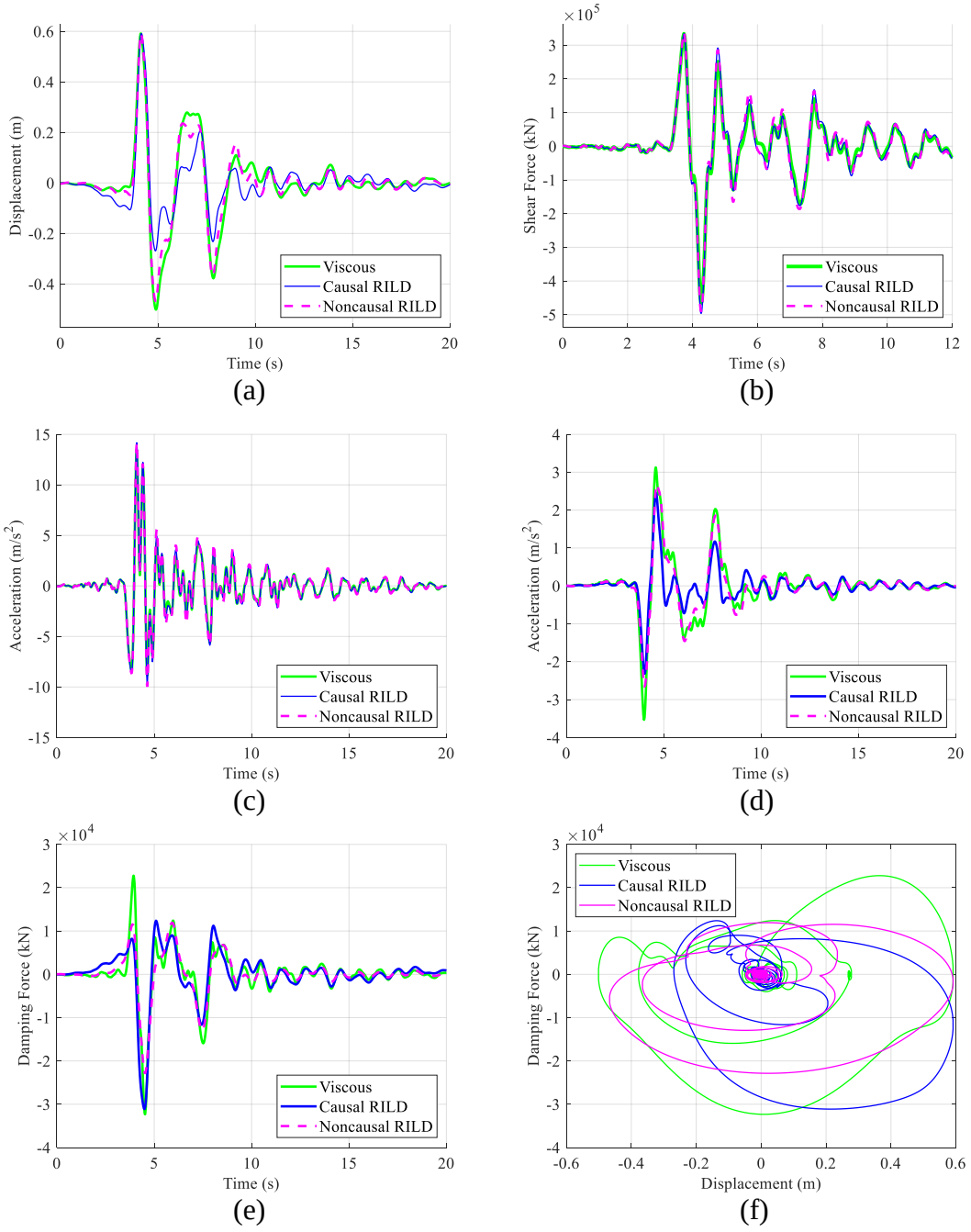

Figure 6.1 RILD Comparison for Northridge Earthquake (a) Inter-story Drift of Isolation Layer (b) Base Shear (c) Absolute Acceleration of 9th Floor (d) Absolute Acceleration of Top Floor (e) Damping Force (f) Damping Force Hysteresis

The outcome of the analysis is a fairly reasonable causal approximation of RILD. The damping force is dependent on the relative displacement of the isolation

layer, as opposed to the velocity, which improves performance for low-frequency excitation, compared to viscous damping. The benefits of lower superstructure acceleration and damping force is maintained with the causal RILD compared to viscous damping, but the causal approximation generally increases the required damping force compared to non-causal RILD.

6.3 Wind

The $c_{viscous}$ and η parameters for the wind analysis were the same as the earthquake analysis in order to analyze the effects of strong winds on an inter-story isolated structure subjected to strong winds. The Adaptive A-D Approach repeatedly sampled the relative displacement and relative acceleration over a period of 10 seconds in order to calculate the dominant response frequency. The results from the simulation and subsequent extreme value analysis procedure in Section 3.5 are given in Table 6.2.

Table 6.2 Causal RILD Peak Response for Wind

Case	Displacement of Isolation Layer (m)	9th Floor Acceleration (m/s^2)	14th Floor Acceleration (m/s^2)	Damping Force (10^3 kN)
Viscous	0.3630	4.17	26.84	1.68
Non-causal	0.2660	5.60	23.70	4.65
Adaptive A-D Approach	0.395	4.76	24.24	4.84
% Difference from Non-causal	75.78%	15.00%	2.28%	4.09%

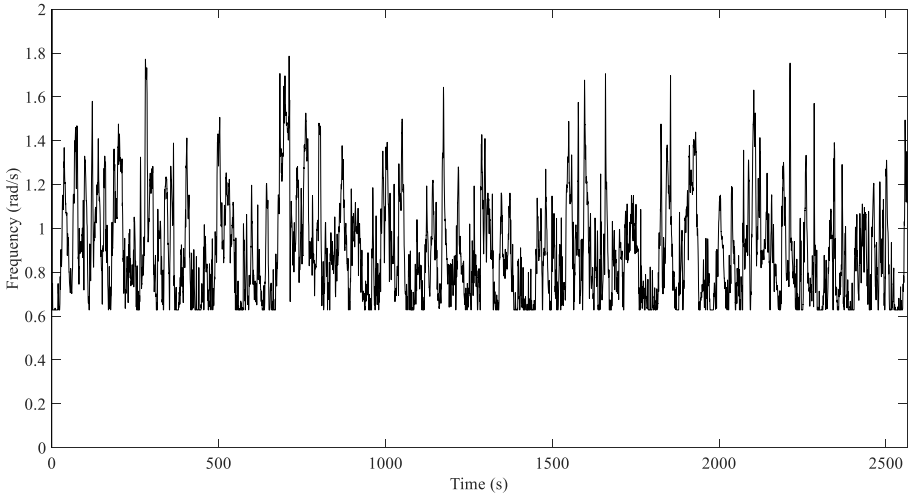

Figure 6.2 Adaptive A-D Calculated Dominant Response Frequency

The results of the Adaptive A-D approach are promising for imitating RILD performance under wind excitation. The frequency of the Adaptive A-D over time presented in Figure 6.2 shows that the dominant response frequency varied between 0.6 rad/s to 1.8 rad/s, the bounds of the algorithm, illustrating the need to implement the adaptive controller as opposed to the single-frequency, CFB approach. This method produces very similar superstructure accelerations for a damping force comparable to that of non-causal RILD. The isolation layer displacement and superstructure acceleration experience a trade-off, so the resulting displacement is higher than that of the non-causal RILD; however, the maximum displacement is still less than half of the isolator diameter, which is an acceptable limit to reduce the risks associated with overturning of the isolators. This confirms that the Adaptive A-D approach can reasonably approximate the benefits of RILD on an inter-story isolated structure subject to strong winds.

Chapter 7: Conclusions

7.1 Conclusion

Inter-story isolation can be used as a multi-hazard protective system. An inter-story isolated system designed for protection against large responses due to earthquake excitation also performs well under wind loading, and has benefits over conventional retrofit in certain cases. When subjected to earthquake loading, conventional retrofit reduces the base shear demand on the foundation, in addition to reducing the floor accelerations of the original structure. This was due to the decrease in fundamental natural frequency of the structure. On the other hand, inter-story isolated retrofit produces base shear and substructure accelerations comparable to that of the original structure, while significantly reducing the floor accelerations of the superstructure. When subjected to strong winds, the conventional retrofit produced lower superstructure accelerations compared to inter-story isolation. The study herein was for a wind event with a 50 year return period, implying that these are not accelerations occupants would experience on a regular basis, and represent a design-case-scenario. Additionally, the large accelerations caused by the low-stiffness layer were able to be improved through supplemental control methods.

Supplemental damping provides a means of reducing large isolation layer displacements under both loading types in addition to reducing the superstructure floor accelerations under strong winds. Adjusting the stiffness of the isolation layer to cause the superstructure to act as a TMD does reduce the peak acceleration of the substructure, but at the expense of higher superstructure accelerations, thereby losing the main benefit of inter-story isolation. RILD was found to reduce the isolation layer

displacement while keeping the damping force and superstructure floor accelerations lower than viscous damping. The main drawback with RILD is that it is a non-causal damping model. A causal filter-based approximation provided reasonable results for earthquake excitation, and an adapted controller provided reasonable results for wind excitation. Implementing an adaptive controller such as the Adaptive A-D approach to replicate RILD at the isolation layer of an inter-story isolated building has potential to be a robust damping method multi-hazard protection system.

7.2 Application

One prominent application of inter-story isolation is retrofitting. Retrofit projects consist of updating a structure to meet a criteria or function it was not initially designed for. This is relevant in major cities where urban sprawl has become a growing concern. Urban sprawl is a phenomenon in which cities expand in an uncontrolled manner (Brueckner 2000), spurring the desire to build cities up vertically as opposed to horizontally. Car-dependent suburban areas decentralize residential, commercial, and retail properties, putting a strain on transportation infrastructure and reducing the efficiency of public transportation networks. Expansive roadways and traffic congestion, among other issues, make urban sprawl something to be avoided. By constructing additions to existing buildings, more commercial and residential space can be built without the environmental impact of new land development, and transportation systems do not have to extend their networks. In turn, this may provide a solution housing for cities' growing population concerns, especially in geographic regions at risk of both earthquake and strong wind events.

When undertaking a retrofit project in regions prone to both earthquake and strong winds, proper analysis of the structure is required not only to ensure the building can support a vertical extension, but also to evaluate the performance of any new protective system. For buildings that are inadequately designed to handle extreme loading cases relevant to their geographic location, sometimes it is more beneficial to retrofit a building to meet current standards or hazards than to demolish and rebuild it. The combination of demolition and new construction can be costly in addition to displacing residents or businesses for long periods of time. Retrofit projects can also include additions to or repurposing of existing structures. This may be relevant when considering protecting structures with historic significance, where a major goal is often tied to preserving culture and history, or when redesigning space to be used more efficiently.

7.3 Future Studies

Recommendations for future studies to expand upon this work are:

- The earthquake analysis in this study evaluated the performance of the structure under three (3) earthquake time histories. Evaluation under a larger earthquake design suite including different return period events is recommended for a more thorough performance evaluation.
- The wind analysis in this study was performed in the along-wind direction. Additional analysis of the structural response in the across-wind direction is recommended for a more comprehensive study.

- Completing this multi-hazard performance analysis for additional inter-story isolation buildings may provide a basis to make general statements about the effectiveness of inter-story isolation as a multi-hazard protective system.

References

Alexander, D., & Alexander. (2011). Earthquakes. In K. Penuel, & M. Statler, Encyclopedia of disaster relief.Thousand Oaks, CA: Sage Publications. Retrieved from http://proxy-um.researchport.umd.edu/login?url=https://search.credoreference.com/content/entry/sagedisrel/earthquakes/0?institutionId=1210

Alexander, D., & Alexander. (2011). Earthquake zones. In K. Penuel, & M. Statler, Encyclopedia of disaster relief. Thousand Oaks, CA: Sage Publications. Retrieved from http://proxyum.researchport.umd.edu/login?url=https://search.credoreference .com /content/entry/sagedisrel/earthquake_zones/0?institutionId=1210

Anajafi, H., & Medina, R. A. (2018). Comparison of the seismic performance of a partial mass isolation technique with conventional TMD and base-isolation systems under broad-band and narrow-band excitations. *Engineering Structures*, *158*, 110-123.

ASCE *Minimum Design Loads for Buildings and Other Structures*. (2010). Reston, VA: American Society of Civil Engineers.

Brueckner, J. K. (2000). Urban sprawl: diagnosis and remedies. *International regional science review*, *23*(2), 160-171.

Burton, M. D., Kwok, K. C., & Abdelrazaq, A. K. (2015). Wind-induced motion of tall buildings: designing for occupant comfort. *International Journal of High-Rise Buildings*, *4*, 1-8.

Chopra, A. K. (2012). Dynamics of Structures Theory and Applications to Earthquake Engineering (4th ed.). Prentice Hall.

Duwadi, S. and Munley, E., "Hazard Mitigation R&D Series: Article 5 - Securing the Nation's Bridges," FHWA-HRT 11-004, 7(6): 2011.

Feng, D., MIYAMA, T., LIU, W., Yang, Q., & CHAN, T. C. (2012). A new design procedure for seismically isolated buildings based on seismic isolation codes worldwide. *Proceedings of 15WCEE*.

Feng, M. Q. (1993). Application of hybrid sliding isolation system to buildings. *Journal of Engineering Mechanics*, *119*(10), 2090-2108.

Gavanski, E., Gurley, K. R., & Kopp, G. A. (2016). Uncertainties in the estimation of local peak pressures on low-rise buildings by using the Gumbel distribution fitting approach. *Journal of Structural Engineering*, *142*(11), 04016106.

Housner, G. W., Bergman, L. A., Caughey, T. K., Chassiakos, A. G., Claus, R. O., Masri, S. F., ... & Yao, J. T. (1997). Structural control: past, present, and future. *Journal of engineering mechanics*, *123*(9), 897-971.

Inaudi, J. A., & Kelly, J. M. (1995). Linear hysteretic damping and the Hilbert transform. *Journal of Engineering Mechanics*, *121*(5), 626-632.

Keivan, Ashkan, Phillips, Brian M., & Ikago, Kohju (2018) Adaptive Causal Realization of Rate-Independent Linear Damping. *Engineering Structures*. (In press)

Keivan, Ashkan & M Phillips, B & Ikenaga, M & Ikago, K. (2017). SEMI-ACTIVE APPROXIMATION OF RATE-INDEPENDENT LINEAR DAMPING FOR THE SEISMIC PROTECTION OF LOW-FREQUENCY STRUCTURES.

Keivan, Ashkan & Zhang, Ruiyang & M Phillips, B & Ikago, K. (2017). Protection of Inter-Story Isolated Structures Through Rate-Independent Linear Damping.

Liu, M. Y., Chiang, W. L., Hwang, J. H., & Chu, C. R. (2008). Wind-induced vibration of high-rise building with tuned mass damper including soil–structure interaction. *Journal of Wind Engineering and Industrial Aerodynamics*, *96*(6-7), 1092-1102.

MATLAB and Simulink version 9.4.0 Natick, Massachusetts: The MathWorks Inc., 2018

Matsagar, V. A., & Jangid, R. S. (2008). Base isolation for seismic retrofitting of structures. *Practice Periodical on Structural Design and Construction*, *13*(4), 175-185.

Murakami, K., Kitamura, H., Ozaki, H., & Teramoto, T. (2000). Design and analysis of a building with the middle-story isolation structural stystem. In *12th World Conference of Earthquake Engineering* (Vol. 857, pp. 1-8).

Ohtori, Y., Christenson, R. E., Spencer Jr, B. F., & Dyke, S. J. (2004). Benchmark control problems for seismically excited nonlinear buildings. *Journal of Engineering Mechanics*, *130*(4), 366-385.

Reggio, A., & Angelis, M. D. (2015). Optimal energy-based seismic design of non-conventional Tuned Mass Damper (TMD) implemented via inter-story isolation. *Earthquake Engineering & Structural Dynamics*, *44*(10), 1623-1642.

Ryan, K. L., & Earl, C. L. (2010). Analysis and design of inter-story isolation systems with nonlinear devices. *Journal of Earthquake Engineering*, *14*(7), 1044-1062.

Sagami, Yoko & Hori, Norio & Ikago, Kohju & Inoue, Norio. (2012). Study on the effect of existence of frequency dependency to damper force of base-isolated structure. Journal of Structural and Construction Engineering (Transactions of AIJ). 77. 529-536. 10.3130/aijs.77.529.

Sueoka, T., Torii, S., & Tsuneki, Y. (2004, August). The application of response control design using middle-story isolation system to high-rise building. In *13th World Conference on Earthquake Engineering*.

Tamura, Y. (2012). "Aerodynamic database of high-rise buildings." ⟨http://www.wind.arch.t-kougei.ac.jp/info_center/windpressure/highrise/Homepage/select_T312_4.html⟩ (March 22, 2018).

Tan, P., Zhang, Y., & Zhou, F. (2008). OPTIMAL DESIGN AND CONTROL MECHANISM STUDY ON STORY ISOLATION SYSTEM. *The 14th World Conference on Earthquake Engineering.*

Vesilind, P. A. (1995). Evolution of the American Society of Civil Engineers code of ethics. *Journal of professional issues in engineering education and practice*, *121*(1), 4-10.

Wang, S. J., Chang, K. C., Hwang, J. S., Hsiao, J. Y., Lee, B. H., & Hung, Y. C. (2012). Dynamic behavior of a building structure tested with base and mid-story isolation systems. *Engineering Structures*, *42*, 420-433.

Zhang, Ruiyang & M Phillips, B & Taniguchi, S & Ikenaga, M & Ikago, K. (2017). PERFORMANCE VALIDATION OF INTER-STORY ISOLATION THROUGH SHAKE TABLE REAL-TIME HYBRID SIMULATION.

Zhou, Y., Kijewski, T., & Kareem, A. (2003). Aerodynamic loads on tall buildings: interactive database. *Journal of structural engineering*, *129*(3), 394-404.